Asian Journal of Nanoscience and Materials 4 (2022) 252-293

Asian Journal of Nanoscience and Materials

Journal homepage: www.ajnanomat.com

Review Article

Understanding the mechanism of electrochemical reduction of CO_2 using Cu/Cu-based electrodes: A review

Pigewh Isa Amos[a], Hitler Louis[b,c], Kayode Adesina Adegoke[d,e*], Ededet Akpan Eno [b]; Akakuru Ozioma Udochukwu[b,f], Thomas Odey Magu[b]

[a] *Department of Chemistry, School of Physical Sciences, Modibbo Adama University of Technology, Yola, Adamawa State, Nigeria*

[b] *Department of Pure and Applied Chemistry, University of Calabar, Calabar, Cross River State, Nigeria*

[c] *CAS Key Laboratory for Nanosystem and Hierarchical Fabrication, CAS Centre for Excellence in Nanoscience, National Centre for Nanoscience and Technology, University of Chinese Academy of Sciences, Beijing, China*

[d] *Department of Chemistry,University of Pretoria, Pretoria, 0002, South Africa*

[e] *Ladoke Akintola University of Technology, Ogbomoso, Oyo State, Nigeria*

[f] *Ningbo Institute of Materials Technology and Engineering, Chinese Academy of Sciences, Zhejiang, China*

ARTICLE INFORMATION

Received: 30 August 2022
Received in revised: 27 September 2022
Accepted: 06 October 2022
Available online: 01 December 2022

DOI: 10.26655/AJNANOMAT.2022.4.2

KEYWORDS

Copper Electrode
Catalyst
Mechanism
CO_2 Reduction
Selectivity

ABSTRACT

Interestingly, copper has been identified as an ideal metal catalyst for an industrial scale electrochemical reduction of CO_2 to various value-added chemicals relative to other metal catalysts reported so far. This is due to the fact that copper and copper based materialshave the potential to convert CO_2 to oxygenates such as ethanol, methanol, formates etc. and hydrocarbons such as ethane, methane etc. Mechanistic details on how these products are formed on the catalystelectrolyte interphase during the reduction process have remained relatively uncovered. This review, therefore, seeks to uncover the mechanism of electrochemical reduction of CO_2 on Cu/Cu based electrodes, factors that affect catalytic activity and selectivity for these electrodes as reported in various literatures. This paper is, therefore, organized as follows: section 1 covers the introduction; an overview of some basic concepts in electrochemical CO_2 reduction (ECR) was discussed in section 2, experimental studies were discussed in section 3, and, finally, we have conclusion

Corresponding author, email: kwharyourday@gmail.com (K.A. Adegoked).

Graphical Abstract

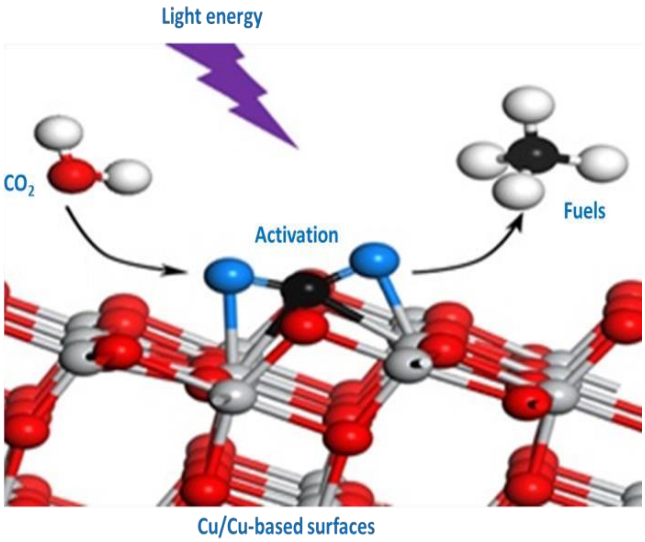

Introduction

Since the industrial revolution of the 19th century, the global trend in technological advancement has always been on the increase, and so is the exploitation of fossil fuels (i.e., coal, petroleum and natural gas) as the main source of energy in order to sustain our economies and societies. These fossil fuels as non-renewable energy sources get depleted on an increasing basis which gives rise to a series of problems [1–3]. On the one hand, the aforementioned advancement, coupled with rapid population growth has resulted to increased energy demand, while fossil fuels as non-renewable resources have very limited reserves, which is gradually leading towards an aggravated energy crisis. Due to the huge consumption of fossil fuels, carbon dioxide (CO_2) as one of the by-product of the combustion of fossil fuels has been constantly emitted and kept accumulated in the atmosphere year by year. Various studies have shown that, the concentration of atmospheric CO_2 as of 22th July, 2017 is as high as 406.38 parts per million (ppm), which far exceeds the threshold safety value of 350 ppm for atmospheric CO_2 [4].This increased in CO_2 levels has been associated with undesirable climatic effects such as global warming, desertification, rising sea levels, and more erratic weather patterns. Therefore, alleviating the effects caused by the heavy CO_2 emission has become a pressing issue to the modern society [5, 6]. Different strategies have been adopted for the reduction of CO_2 emission and mitigating climatic change which include; the use of clean renewable energy sources such as solar, wind and tide in place of fossil fuels, and direct capture and sequestration of CO_2 for a long time isolation from the atmosphere ("carbon capture and Storage" CCS) [7–10].

The captured CO_2 emissions can also be considered as a valuable resource because CO_2 can be catalytically converted into industrially relevant chemicals and fuels. This is an extremely attractive approach since it can reduce the carbon footprint associated with fossil-fuel-powered processes, thus allowing the sustainable use of current fossil-fuel resources, and generate revenue to offset the costs associated with other CO_2 capture,

storage, and transport efforts. Several methods have been proposed for the conversion of CO_2 to value added chemicals; however, thermochemical, photochemical, and electrochemical CO_2 conversion are all promising catalytic approaches [11]. Electrochemical CO_2conversion technologies are appealing because they operate with high reaction rates and good efficiencies under ambient conditions, use environmentally benign aqueous electrolytes, easily couple with carbon-free electricity sources (e.g., wind, solar, hydroelectricity, etc.) and the reaction rate can be controlled easily by tuning the external bias (i.e.,overpotential) [12]. Another benefit of electrochemical CO_2 conversion is that several voltage-dependent products are accessible, including formic acid, carbon monoxide, methane, and ethylene etc. [13, 14]. Although the electrochemical reduction of CO_2 to valueadded products has promised the high overpotential of this reaction, low selectivity and production rate, however, activity of the currently known catalysts still hampers this process from becoming close to commercialization. This is backed by the fact that typical current densities have been in the order of milliamps per square centimeter (mA/cm^2) of electrode and catalyst surface whereas industrial water electrolyzers operates at the magnitude of $2A/cm^2$ [15, 16]. Current researches in this field are aimed at obtaining an ideal catalyst, capable of electrochemical conversion of CO_2 at an industrial scale with improved efficiency, low overpotential and high selectivity towards a particular product. In this way, CO_2 electrochemical reduction to liquid fuels and other valueadded chemical feed stocks could become a sustainable way to store chemical energy in liquid forms.

Studies have shown that several metallic elements such as Cu, Au, In, Sn, Pb, Zn, Ag, Pd, Bi and Carbon based materials are catalytically active for the electrochemical CO_2 reduction in aqueous electrolytes [17–27]. However, several factors have been identified to affect the yield and type of products obtained during electrochemical reduction of CO_2. These factors include; the type, nature and morphology of the metal electrode used as the catalyst, the type of electrolyte used, the medium in which the reaction was conducted, the applied potential and reaction conditions such as temperature and pressure. These aforementioned metals with catalytic activity for the reduction of CO_2 are grouped into three classes based on the major products obtained during their electrochemical reaction. Elements such as Sn, Hg, Pb, and In, etc., are classed as group 1 metals because they generate formate or formic acid as their main products [21]. Au, Ag, Zn, and Pd are typical representatives of the group 2 metals whose predominant reaction product is CO [15, 16], whearas Cu is a representative of the group 3 family and greater attention is given to Cu/Cu-based materials because it is the only catalyst known to electrochemically convert CO_2 to hydrocarbons and/or oxygenates such as ethanol at considerably high Faradaic efficiency (FE)[28]. Intensive research efforts, both experimental and theoretical have focused on improving the overpotential and selectivity of Cu-based catalysts for the electrochemical reduction of CO_2 to specific products. Among the range of value-added chemicals into which CO_2 can be reduced to, ethanol and hydrocarbons receives more attention because of their economic importance and application as alternative sources of fuels (biofuels) other than fossils, they can also serve as feed stocks for various chemical industries.

Several quality reviews have been published which discussed the catalytic conversion of CO_2 to value added chemicals on various metal catalysts. However, few among such reviews were dedicated to Cu and Cu-based materials.

This review, therefore, seeks to dig deep into the world of Cu/Cu related catalysts in order to understand the mechanism of electrochemical reduction of CO_2 taking into account, the effects of electrolytes, morphology of the catalysts, nature of the crystallites, effects of functional groups, surface modification, grain boundary, effects of cocatalysts, Cu overlayers, effects of product selectivity and many more.

The table presented in this review has been constructed using data from various sources. We have made as much effort as possible to present the data in a way that is useful to the reader, allowing one to compare results from different research groups, based on published results from various sources to generate all the relevant data. The quality of the published data, however, varied quite a bit and we had to make judicious choices in selecting relevant and reliable data.

An Overview of Some Basic Concepts in Electrochemical CO_2 Reduction (ECR)

Before delving deep into the world of electrochemical reduction of CO_2 to value-added chemicals on Cu and Cu-based materials, one needs to understand the fundamentals of this unique chemical process. Below is a brief overview of some important concepts used in the study of ECR:

Chemical/Thermodynamic stability of CO_2

Carbon dioxide (CO_2) is a linear and nonpolar molecule, fully oxidized and extremely stable molecule. Inducing a chemical conversion from this stable state requires efficient and robust electrocatalysts to promote this kinetically sluggish reduction process. Therefore, a real-world catalysts often require large overpotentials (as can be seen where a single-electron reduction of CO_2 to form $CO_2^{\bullet-}$ require as high as -1.9 V vs RHE reduction potential; this high value is due to the rearrangement of the molecule from a linear to a bent structure.), to promote the reaction at satisfactory rates and product selectivity. The energy needed for CO_2 conversion should arise from sustainable low-carbon sources (e.g. solar, wind, tidal energy etc.) in order to have an impact on atmospheric CO_2 concentration. The major challenge therefore, is to fabricate an electrocatalyst that can achieve high conversion efficiency, high product selectivity at low overpotential barrier.

Reaction Mechanism of ECR

The mechanism for electrochemical CO_2 reduction has been studied for many years, with the typical aim of the research being directed towards understanding why different metals give different products. Researchers across the world have proposed and continue to propose novel reaction pathways for ECR based on their understanding of CO_2 reduction on metallic electrodes

Electrochemical reduction of CO_2 is a multi-step reaction process generally involving two, four, six, or eight-electron reaction pathways [29], which often take place at the electrode-electrolyte interface, where the electrode is a solid electrocatalyst while the electrolyte is usually an aqueous solution saturated with CO_2. Typically, this catalytic process involves three major steps:

i. Chemical adsorption of CO_2 on an electrocatalyst
ii. Electron transfer and/or proton migration to cleave C–O bonds and/or form C–H bonds
iii. Configuration rearrangement of products to desorb them from the electrocatalyst surface and diffuse into the electrolyte [30].

The electrocatalyst employed and the electrode potential applied has a great influence

on the final reduction products. In general, the reaction products are a mixture of carbon compounds with different oxidation states, and they often include carbon monoxide (CO), formate ($HCOO^-$) or formic acid (HCOOH), methane (CH_4), ethylene (C_2H_4), ethanol (C_2H_5OH), methanol (CH_3OH), etc [31, 32]. Since ECR is a surface phenomenon, there is no generalized reaction pathways towards the products obtained. In fact, the mechanism of the reaction must depends on the type, nature and morphology of the catalyst, the catalyst's relative selectivity towards a particular intermediate (i.e. the relative ease with which a catalyst adsorbs and desorbs an intermediate), the number of electrons transferred and the energy barrier required for this electron transfer (standard reduction potential) as demonstrated by the sets of equations in the Table 1.

Table 1. List of Several ECR reaction products, the $CO_2^{\bullet-}$ intermediate, and the H_2 evolution reaction with their reaction mechanisms and standard reduction potentials (E^o) [33]

Products	Reaction	E^o(V vs. RHE)
CO	$CO_2 + 2e^- + 2H^+ \rightarrow CO + H_2O$	-0.11
HCOOH	$CO_2+2e^- +2H^+ \rightarrow HCOOH$	-0.25
HCOH	$CO_2+4e^-+4H^+ \rightarrow HCOH+H_2O$	-0.07
CH_3OH	$CO_2+4e^-+4H^+ \rightarrow CH_3OH+2H_2O$	0.02
CH4	$CO_2+8e^- +8H^+ \rightarrow CH_4+2H_2O$	0.17
C2H6	$CO_2+12e^-+12H^+ \rightarrow C_2H_4+4H_2O$	0.06
$CO2^{\bullet-}$	$CO_2+e^- \rightarrow CO_2^{\bullet-}$	-1.5
H2	$2H^+ +2e^- \rightarrow H_2$	0.0

As stated earlier, the electrochemical CO_2 reduction reaction (CO_2RR) occurs in three steps. The first step involves oneelectron transfer to CO_2 to form a key intermediate $CO_2^{\bullet-}$, which is the rate limiting step in the reaction, largely due to the structural rearrangement from a linear molecule to a bent radical. This requires an enormous amount of energy usually, an overpotential of -1.9V vs. RHE is needed in order to promote this kinetically sluggish reduction process at a satisfactory rate. After the first step, the obtained $CO_2^{\bullet-}$ which is very reactive undergoes several proton-coupled multiple-electron-transfer reactions, which are thermodynamically more favourable and takes place almost instantaneously.

Some important parameters used in the study of CO_2RR

CO_2 Reduction Efficiency

There are two distinct types of efficiencies, Faradaic efficiency (FE) and Energy efficiency.

Faradaic efficiency is quite simple to calculate and understand: it is the percentage of electrons that end up in the desired product. In other words, it is defined as the percentage of electrons consumed for the formation of a given product and can simply be expressed as:

$$E_{faradaic} = \frac{\propto nF}{Q}$$

Where, α is the number of electrons transferred, n is the number of moles of the target product, F is the Faradaic constant and Q is the quantity of charge consumed or passed.

On the other hand, the Energy Efficiency is the amount of energy in the products divided by the amount of electrical energy put into the system which is the overall energy utilization of the system and can be expressed as:

$$E_{energetic} = \frac{Eeq}{Eeq \times \eta} \times E_{faradaic}$$

Where, E_{eq} is the equilibrium potential and η is the overpotential

Overpotential

This the difference between the applied potential (onset potential) versus the reference electrode under which the desired product is yielded at a detectable amount, and the standard reduction potential *(E^o)* which is given as $\eta = (E_{applied} - E^o)$.

Current density

Current density for CO_2 reduction is the ratio of the magnitude of current to the geometric surface area of the working electrode. Partial current density for specific products can be obtained by multiplying the corresponding FE by the overall current density.

Experimental studies

As stated earlier, Cu is the only metal catalyst that shows catalytic activity towards electrochemical reduction of CO_2 to variety of hydrocarbons and alcohols. This uniqueability therefore makes Cu and Curelated catalysts to be seen as ideal materials to be used for commercial and/or industrial CO_2 conversion to value-added chemicals in order to solve energy and environmental problems arising from excessive atmospheric accumulation of CO_2 gas. Researchers around the globe have dedicated their time, energy and resources, exploring novel materials and structures as well as the dynamics of this catalytic process on the metal surfaces. Even though this area of research is still growing and the current progress recorded is still far from commercialization, the useful contributions of these researchers and their findings are making headway for the future, and some of these findings shall be discussed in this section taking into consideration, the mechanisms of their electrochemical reduction and the factors that affects the selectivity, improved overpotential and faradaic efficiency of the products obtained.

Cu/Cu-based catalysts for CO_2RR

Loiudice *et al* fabricated Cu Nanocrystals (NCs) used for CO_2RR [34]. Their study reveals a structure/property relationship between the fabricated Cu Nanocrystals and their catalytic activity (Figure 1). The selectivity over hydrogen evolution reaction (HER), and activity of the NCs towards C_2 products predominantly C_2H_4, depends on the morphology as well as the size of the nanocrystals. Within the same morphology, smaller NCs exhibited higher activity; however, overall, the cube-shaped NCs where more intrinsically active than the spheres. The Cube-shaped NCs (24 nm, 44 nm, and 63 nm sized NCs) shows a nonmonotonic size-dependent selectivity in which the 44 nm cube-shaped NC exhibited the best catalytic performance with 80% efficiency towards selectivity of CO_2RR over HER and FE of 41% for C_2H_4 as shown in Table 2. This recorded selectivity was attributed to the presence of active sites on the surface of the Nanocrystals (plane, edge and corner). The X-ray Diffraction pattern (XRD) reveals that the (100) plane facets predominate on the surface as shown in the model used in Figure 1. As the size of the Nanocubes increases, the relative number of atoms on the edges and the corners decreases while the number on the planes increases. This therefore results into a surface configuration closer to one single crystal with all the surface atoms lying in the (100) plane. The studies concluded that, since uncoordinated sites in nanocrystals such as corners, steps, kinks, etc. favours HER selectivity, the trends of the Cu nanocubes towards coordinated (100) plane

sites are responsible for the improved CO_2RR selectivity. This active site/size trend suggests that the unique reactivity of the 44 nm Cu NC cubes derives from an optimal balance between plane and edge sites, while the edges are responsible as ethylene-selective active sites in the Cu NC cubes.

Song and co-workers [35] reported the catalytic activity of Cu Nanocrystals on a highly textured N-doped Carbon nanospikes (Cu/CNS) with selectivity of 84% and the FE of 63% at -1.2V vs RHE for ethanol production (Table 2). Here, Cu/CNS exhibited unsual behaviour because it favours ethanol formation rather than methane and ethylene; this is because ethanol requires C-C coupling between surface-adsorbed intermediates at some points during the reduction reaction. This high selectivity for C2 product suggests that C-C coupling was preferred to desorption of the C1 intermediate.

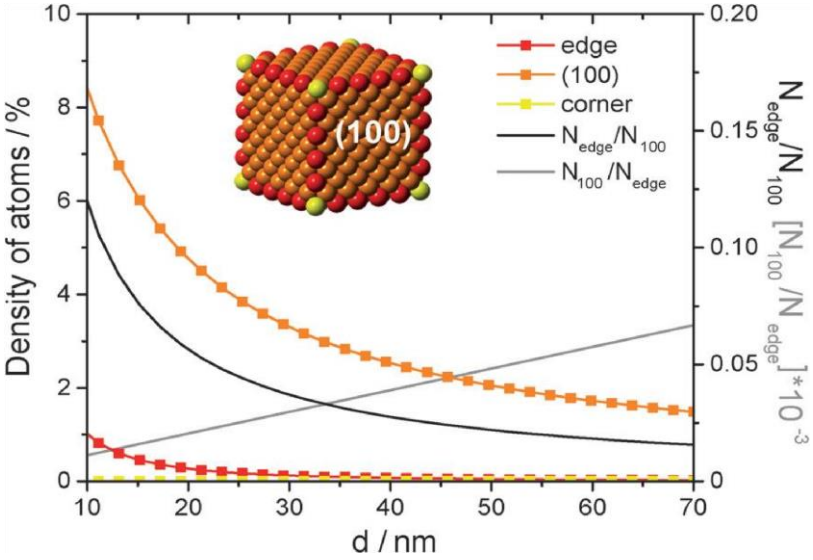

Figure 1. On the left axis: Density of adsorption sites in Cu NC cubesreported versus the edge length (d). On the right axis: trend of N_{edge}/N_{100} and N_{100}/N_{edge} versus d, where N_{edge} is the number of atoms atthe edge and N_{100} is the number of atoms on the (100) plane [34]

This preference was suggested to be as a result of the nanostructured nature of the surface which improves the stability of the adsorbed C_1 intermediate keeping it long enough until a second intermediate is available for C_2 coupling. The coupling reported could be between two surfaces bound intermediates or between surface bound intermediate and a nearby C_1 intermediate in solution. Furthermore, the ethanol production dominates the competitive reduction of the coupled C_2 to ethylene or methane. This unique behavior was reported to be as a result of electronwithdrawing effects in the graphene πconjugated system, which in turn, polarizes the carbonatoms adjacent to nitrogen positively. This polarization was suggested to provide an active site adjacent to the copper for the C_2 intermediates to adsorb, which may inhibit complete electroreduction. Density Functional Theory (DFT) calculations performed by the group also suggested that the strongly curled morphology of the CNS aids in the adsorption of C_2 intermediates. CNS reported in their study was puckered curled, indicating local corrugation on the surface. Such local deformation and curvature naturally

embedded into the CNS could help in strengthening the bond between C_2 and CNS.

Moreover, Song and co-workers [35] also studied the interaction between C_2 intermediates (OCCO) and the Cu surface; they found out that there is a strong covalent bond when the molecule approaches the Cu surface oriented with one end closer to the surface. This covalent bond is comparatively stronger than the OCCO/NCS bond which ensures that desorption of C_2 intermediates are prevented, the group therefore proposed that, the C_2-intermediates is covalently bound on reactive copper surface for complete reduction to $-CH_3$, while the oxygen atomon the other end of the C_2intermediates is adsorbed on less reactive CNS hence forming $-CH_2OH$, and protected from competitive reduction, thereby providing a pathway towards selective reduction to ethanol.

Zhiyuan *et al* [36] reported highly selective reduction products on Ag@Cu Bimetallic catalyst. The group fabricated an Ag@Cu core-shell system whose nanoparticles were controlled by tuning the heating reaction time in a simple polyol reduction method (0-20 mins) and the following were obtained Ag@Cu-5, Ag@Cu-7, Ag@Cu-10, Ag@Cu-15, Ag@Cu-20, Ag@Cu-25 respectively (i.e. Ag@Cu-reaction time). The peak activity was recorded at Ag@Cu-7 for CO generation whose FE was 82% and decreases dramatically to 20% for Ag@Cu10, while Ag@Cu-20 gave a peak FE of 28.6% for C_2H_4 (Table 2), as this clearly demonstrates that Ag@Cu-7 (Ag-dominant) and Ag@Cu-20 (Cu-dominant) bimetallic materials achieved better activities for CO_2RR than other counterparts. The authors pointed out that there exist a composition and structure dependent activity and selectivity in the series of the as-prepared Ag@Cu bimetallic catalysts, and that geometric effects rather than electronic effects was the key factor in determining the selectivity. The peak activity at Ag@Cu-7 towards CO as suggested, resulted from functional Ag (modified) with more oxygen affinitive Cu via oxygen-metal interaction which helped to stabilize *COOH intermediate, a key point to lower the energy requirement for CO_2RR and gain higher FE towards CO. Furthermore, the small amount of Cu for Ag@Cu-7 cannot offer the possibility to stabilize of *CO intermediate to protonate successively to hydrocarbons. Conversion to ethylene came as a result of the increase in Cu content at Ag@Cu-10 and above. It was concluded that, synergistic reactions rather than pure dilution effects between Ag and Cu for these AgCu bimetallic electrocatalysts mainly derived from the mixing pattern of the components played an important role in producing the higher CO or hydrocarbons. Ma and co-workers [37] reported

Cu-Pd bimetallic catalysts with different mixing patterns used for the electrochemical reduction of CO_2. Their study examines a range of bimetallic Cu-Pd catalysts with ordered, disordered, and phase-separated atomic arrangements (Cu_{at}:Pd_{at}=1:1), as well as two additional disordered arrangements (Cu_3Pd and $CuPd_3$ withCu_{at}:Pd_{at} =3:1 and 1:3). The result reveals high selectivity for C_1 products(mainly CH_4) in the ordered structure while the phaseseparated and the Cu_3Pd exhibited high selectivity for C_2 products (Table 2) where the following cases were observed; CO is an important precursor for C_2 chemicals production and the phase-separated CuPd catalyst converts adsorbed CO to C_2 chemicals more easily than the ordered CuPd catalyst, with latter converting adsorbed CO more easily to CH_4 than the phase-separated catalyst. The high selectivity of the phase-separated CuPd structure for C_2 products was as a result of dimerization of adjacently adsorbed CO to COCOH intermediates due to interacting neighbouring features of Cu atoms with

favourable molecular distances between them and small steric hindrance (Fig. 2). Similarly, the preference for CH_4 on the ordered-CuPd (Fig. 2) structure was due to presence of Cu-Pd intermetallic structures which adsorbed CO on a Cu and further converted it to CHO intermediate whose oxygen atom is partially adsorbed to Pd atom which stabilizes the adsorption of CHO intermediate and favours the production of CH_4. The study also reveals that, as the concentration of Cu increases from Pd, $CuPd_3$, CuPd, to Cu_3Pd and Cu, the FEs for C_2 products also increased which further supported the idea that the dimerization of adsorbed CO to form C_2 chemicals may be preferred on the sites with neighboring Cu atoms. The group implies that the selectivity of different therefore concluded that the selectivity of products can be tuned by altering the the Cu-Pd bimetallic catalyst can be geometric arrangements of the catalyst.

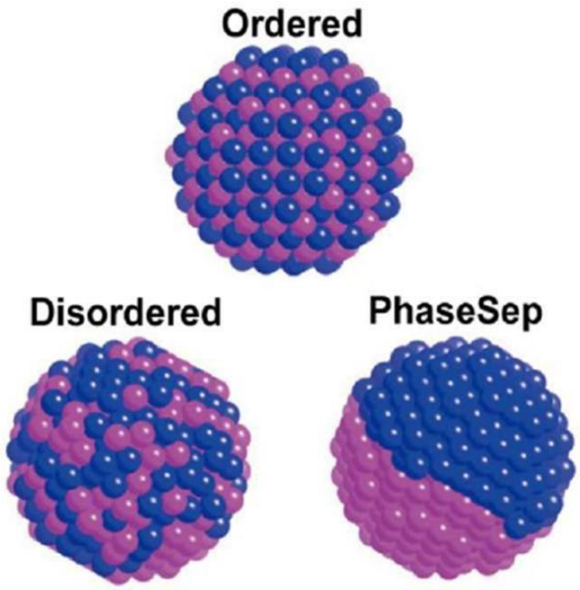

Figure 2. Schematic illustration of prepared CuPd Nanoalloys with different structures [37]

Lum *et al* [38] reported that trace levels of copper in carbon shown significant electrochemical CO_2 reduction activity. The study investigated the catalytic activities of pure graphite (PG), graphene oxide (GO), and carbon nanotubes (CNT) dispersed on glassy carbon (GC) for the electrochemical CO_2 reduction reaction in aqueous solution (Table 2). It was observed that carbon support materials exhibited significant electrocatalytic behaviours attributable to the presence of impurities in them. However, the presence of Cu as impurity in GO configuration revealed a significant yield of methane. Interestingly, it was revealed that the catalytic activity of the GO-supported material dropped significantly when nearly all the impurities were washed away in ultrapure nitric acid. On re-introduction of Cu, the catalytic behavior surfaced which increases with increase in the amount of Cu deposited. On comparison between Cu electrodeposited on GO/GC, PG/GC and GC systems, it was revealed that the activity per mass of Cu is ~ 4-5 times higher for GO/GC or PG/GC than GC, attributable to preferential deposition of Cu-NPs at defects present on the graphene layers of GO and PG with latter having the highest activity for methane production

(Table 2). The group therefore suggested that, a highly active catalyst for methane formation via the CO_2RR can be created for the future by the introduction of defects into graphene layers, onto which Cu can then be electrodeposited.

Hahn and co-workers [39] studied the surface structure of Cu thin films catalysts in order to probe the relationship between active sites and catalytic activity for the electroreduction of CO_2 to fuels and some value added chemicals. In their study, they reported a vapor deposition of Cu thin films on large-format single-crystal substrates (Al_2O_3(0001), Si(100), and Si(111)), and confirm epitaxial growth in the (100), (111), and (751) orientations respectively (Fig. 3). Results of electrochemical CO_2 reduction reveals that the three orientations all make > $2e^-$ reduction products in the tested potential range between −0.89 and −1.10 vs. RHE. However, Cu(100) and Cu(751) are both active and selective for C-C coupling reaction than Cu(111) and Cu(751) is the most selective for the > $2e^-$ oxygenate formation at low overpotential. The group pointed out that the difference in selectivity could be due to due to a lower kinetic barrier for CO dimerizationon Cu(100) compared with Cu(111). This therefore suggest that there is a

strong correlation between C–C coupling selectivity and the coordination number of the surface, which was favoured by the less coordinated Cu(100) and Cu(751) than the more coordinated Cu(111) (Fig. 3).

On the other hand, analysis of oxygenate vs. hydrocarbon selectivity was conducted on the three orientations and they came to a conclusion that at −0.89 V vs. RHE, Cu(751) has the highest oxygenate/hydrocarbon ratio, and the group put forward a suggestion that this improvement in oxygenate selectivity is related to the fewer number of nearest neighbors on the Cu(S)–[n(110) × (100)] (*in-situ* surface structure of Cu (751) where 'n' varies from 2 to 7) surface, or the top most layer of the Cu (751) film, because barriers for hydride transfer are predicted to be lower than those for proton-coupled electron transfer at lower overpotentials.

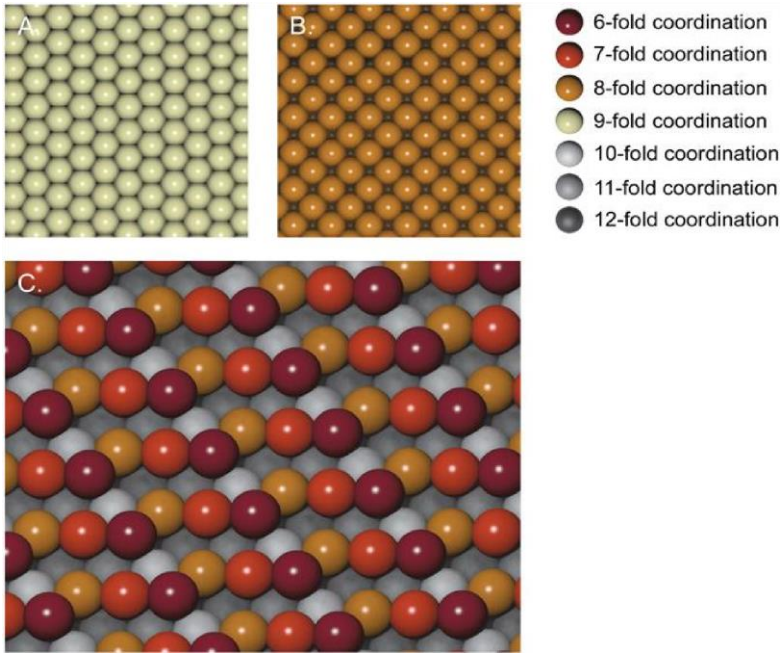

Figure 3. Color-coded atomic models showing coordination numbers for the (A) Cu(111), (B) (100), and (C) (751) surfaces [39].

Zhang *et al*. [40] investigated CO_2 electroreduction on Cu overlayers on tetrahexahedral Pd nanocrystals (THH Pd NCs) with (310) high-index facets. The study revealed catalytic activity/selectivity towards alcohols (ethanol and methanol). Cu_{1ML}/THH Pd NCs exhibited high activity and selectivity for CO_2electroreduction to ethanol with ~20% FE at -0.46 V vs. RHE. The selectivity of the alcohol was readily tuned by varying the coverage of Cu on THH Pd NCs in which methanol was obtained at $Cu_{0.8ML}$/THH Pd NCs with FE of 19.5% (Table 2). According to the group, the results demonstrated that the electroreduction of CO_2 is a surfacestructure-sensitive reaction and the (310) high-index facets facilitate the formation of ethanol.

Mixed iron-copper (Fe-Cu) oxide catalyst was reported by Yang *et al*. [41] for the electrochemical reduction of CO_2 to acetate with FE of 80% and 76% using Arpurged, phosphate-buffer and $NaHCO_3$ electrolytes respectively (Table 2). The catalyst reported here is a mixed phase material consisting $CuFeO_2$ and CuO. The study reveals that competing production of formate over the mixed structure existed which was favoured by the increase in concentration of Cu relative to Fe. Here, the selectivity of the catalyst towards either acetate which is the primary product or formate is a function of the iron-copper atomic ratio represented as Fe:Cu. At a ratio of 1:3, the catalyst favours the production of acetate but as the concentration of Cu increases relative to Fe from 1:3 through 0:5, and 0:1, the products obtained was predominantly formate. This result therefore suggested that varying the Fe:Cu atomic fractions, the selectivity of the catalyst can be tuned from primarily acetate to primarily formate. Furthermore, the morphology of the as-prepared catalysts is also a function of their composition which was reported that the grain size decreases slightly as a function of increasing Fe:Cu ratio.

Copper nanofoams with hierarchical porosity was investigated for the electrochemical reduction of CO_2 [42]. This study reveals an improved product distribution and faradaic efficiency which far exceed the one obtained from smooth electropolished Cu-electrodes (Table 2). This result was attributed to high surface roughness, hierarchical porosity, and confinement of reactive species.

Oxide-derived Cu_xZn catalysts was reported by Ren *et al.* [43], used for the electrochemical reduction of CO_2. Where Cu_xZn = $Cu_{10}Zn$, Cu_4Zn, and Cu_2Zn. Cu and its oxides are used to demonstrate that the selectivity of CO_2 reduction to ethanol could be improved by introducing a cocatalyst to generate an *in-situ* source of mobile CO reactant, achievable by doping the Cu-based oxides with varying amounts of Zn dopants. This observation was also accountable for tuning the selectivity for the production of ethanol over ethylene by a factor of ~12.5. Peak production of ethanol was recorded on Cu_4Zn at −1.05V vs RHE, with a faradaice fficiency of 29.1% and a partial current density of −8.2 mA/cm^2 (Table 2).

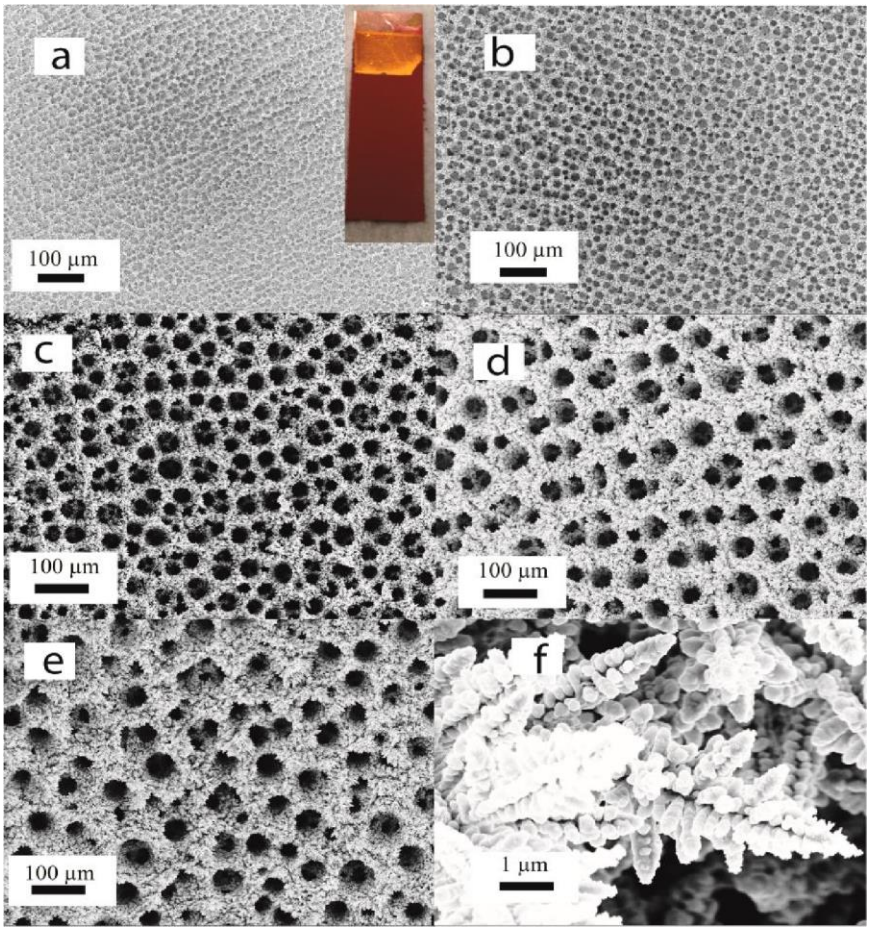

Figure 4. SEM images of electrodeposited copper foams on a copper substrate for (a) 5s; (b) 10s; (c) 15s; (d) 30s; and (e) 60s; (f) nanostructure of the electrodeposited foam [43].

The formation of ethanol and ethylene on Cu_xZn surfaces could be as a result of synergistic interaction between Cu and Zn which promotes the formation of ethanol. The group therefore postulated that, gaseous CO formed from the Zn sites may have further reacted to give ethanol. This postulation was strengthened by the observation that the potential where the FE of ethanol had peaked shifted to a more negative value on Cu_4Zn, and Cu_2Zn in comparison to Cu catalyst. This is because the CO needed for enhanced ethanol formation could only be generated in greater quantities on the Zn sites at more cathodic potentials. They also proposed in the mechanism of reaction that, for ethanol to be produced on a roughened surface (Fig. 4) such as Cu_xZn, CO is needed for insertion into the bond between into the bond between Cu and $*CH_2$ to form $*COCH_2$, whose further reduction yields acetaldehyde and finally ethanol.

Similarly, selective electrochemical CO_2 reduction to ethylene and ethanol on copper (I) oxide catalysts was investigated by Ren and co-workers [44]. They reported that the Faradaic yield for both ethylene and ethanol can be systematically tuned by changing the thickness of the deposited overlayers. Peak selectivity was observed for the film thickness of 1.7–3.6 µm at –0.99 V vs RHE, with faradic efficiencies (FE) of 34–39% for ethylene and 9–16% for ethanol (Table 2). This selectivity was

optimized according to material analysis, with the 1.7−3.6-μm-thick films, which consisted of 0.5−1-μm-sized Cu polyhedron particles. They also proposed that during the the CO_2 reduction, stepped surfaces with edges and terraces are likely to be formed as copper (I) oxide reduce to metallic Cu. Therefore, the optimum combination of these features must be necessary to dissociate CO_2 and to optimize the chemisorption energies of the CH_xO intermediate. Edeges with undercoordinated Cu atoms plays a vital role in promoting the build-up of a large coverage of CH_xO reactive intermediates, to facilitate their dimerization. The study was concluded that variation of the local pH at the surface of the catalyst was also a factor that boosted the calalysts' selectivity; however, higher selectivity was attributed to step and edge morphological features of the catalysts.

Recently, Reller and co-workers [45] reported nano dendritic Cu catalysts which were selective for the electrochemical reduction of CO_2 towards ethylene at high current density. The result reveals a 57% FE for ethylene and a current density of 170 $mAcm^{-2}$ (Table 2). The dendritic structure consists of mainly Cu and Cu_2O. The i*n-situ* deposition of Cu in acidic pH environment forms the catalytic layers which enables the selective formation of ethylene. It was also revealed that, the catalytic performance of the material does not depend on the supportted material [45]. Furthermore, structural changes of the active sites were observed during the electrolysis such as sintering and/or dissolution/re-deposition and oxidation of the Cu, results to structural degradation and coarsening of the initially formed active species. This leads to the lost of the much required high index facets with low coordinated sites responsible for the formation of ethylene, thereby, creating new catalytic centers having lower hydrogen overpotential which favours the formation of hydrogen.

Recently, Cu/SnO_2 core/shell structure was reported by Li *et al* [46], used for the electrochemical reduction of CO_2 to CO. During the reduction, thin layer of SnO_2 was coated on Cu-nanoparticles. It was observed that, the reduction was Snthickness dependent. About 1.8 nm thick shell shown Sn-like activity to generate formate while the thinner 0.8 nm shell is selective to the formation of CO with the conversion Faradaic efficiency reaching 93% at -0.7V vs. RHE (Table 2). Their study proposed that the formation of CO by the 0.8 nm thick SnO_2 shell could be as a result of alloying with trace of Cu which causes a morphological change such that, the SnO_2 lattice become uniaxially compressed and also, the tinted contamination of SnO_2 with Cu, favours the formation of CO over formate. Therefore, synergistic effects between Cu and SnO_2 in the core/shell Cu/SnO_2 structure as explained above, accounts for the preference and could be used to tune the selectivity of electrochemical CO_2 reduction towards CO products.

The yield behavior of an electrodeposited cuprous oxide thin film was examined by Le *et al* [47]. The study explored the relationship between surface chemistry and reaction behavior of the aforementioned material system, relative to air-oxidized and anodized Cu electrodes.

Higher yield and faradaic efficiency (38%) for CH_3OH was observed at Cu (I) active sites as compared to air-oxidized and anodized Cu electrodes (Table 2). This suggested that, Cu (I) active sites might have played a vital role in the catalyst's selectivity to CH_3OH. The results also, revealed that at the required potentials for CO_2 reduction, copper oxides are reduced to metallic Cu and the products yields are dynamic. Furthermore, it was revealed that the Cu (I) active specie might be responsible for

improving the stability of the intermediates, and enhance the selectivity towards CH_3OH by enabling hydrogenation of oxygen atoms from H_3CO adsorbates.

Ke and co-workers reported a CuOderived porous copper nano-ribbons array [48], used to electrochemically convert CO_2 to C_2 products. At applied potential of −0.701V vs RHE, the C-C coupling reaction is favoured whose total faradaic efficiency towards the formation of C_2H_4, C_2H_6 and C_2H_5OH reached up to ~40% (Table 2), while suppressing the formation of C_1 products. The authors therefore established the preference for C_2 products over C_1 products can be attributed the presence of surface defects and large number of grain boundaries on the CuO-derived copper nanoporous ribbon arrays. The roughened porous channels of these electrodes allowed for facile diffusion of electrolyte and provided large number of active step sites for CO_2 reduction.

Similarly, electrochemical CO_2 reduction on Cu_2O-derived copper nanoparticles was studied by Kas *et al* [49], by controlling its activity towards hydrocarbon production. In this report, selectivity of the CO_2 electroreduction was found to depend largely on Cu_2O film thickness, rather than on the initial crystal orientation. This was due to the fact that the Cu_2O reduction itself seems to be highly favoured relative to the CO_2 reduction or water splitting. Therefore, the catalytic behavior was predominantly due to the layer thickness associated with local pH changes, thus impacting the hydrocarbon selectivities. The group therefore suggests that optimum number density of nanoparticles with the combination of the right electrolyte (pH) can open up routes for highly selective ethylene formation via electrochemical CO_2.

Hossain and co-workers performed the electrochemical reduction of CO_2 using copper/reduced graphene oxide nanocomposite catalysts (Cu-rGO) [50]. The study reveals a catalyst which could effectively reduce CO_2 to CO, HCOOH and CH_4 with a faradaic efficiency of 76.6% at 0.4V vs RHE and excellent stability (Table 2). Uniformly distributed small Cu nanoparticles on the rGO and the synergistic coupling effect of the formed nanocomposite were responsible for the superior electrocatalytic activity and stability of the Cu-rGO nanocomposite achieved. The electron transfer between the rGO and Cu nanoparticles might have increased localized electron concentrations, resulting in significant enhancement of the catalytic activities of the nanocomposite for the electrochemical reduction of CO_2.

In a research work conducted by Hoang *et al* [51], nano porous copper films were fabricated by additive-controlled electrodeposition (i.e. 3,5-diamino-1,2,4triazole (DAT) as an inhibitor), used in CO_2 reduction catalysis. By varying different synthesis parameters such as pH and deposition current density, the morphologies of the thin films are tuned into dots, wire and amorphous structures. The wired structure exhibited the best catalytic activity with high faradaic efficiency for C_2H_4 product as reported in Table 2. The Cu films were reported to produce active sites i.e. small and stable pores which allow for gas permeability thereby, making the resulting structures tunable depending on the deposition conditions. On the same vein, the preference of the Cu-DAT wire structure for C_2 over C_1 products was reported to be as a result of the presence of steps and edges with low coordinated Cu atoms which promotes the adsorption of C_1 products and its subsequent dimerization to C_2 products.

The underlying causes for the selectivity of CO_2 electroreduction toward ethylene on Cu_2O-derived Cu catalysts were studied by Handoko *et al* [52]. They reported that there exist, an inverse relationship between the crystallite

sizes of the Cu_2O-derived Cu particles and the selectivity of the CO_2 reduction towards C_2H_4. Interestingly, decrease in the particle's crystallite size from 41 to 18 nm, results in an increased Faradaic efficiency (FE) of C_2H_4 formation increased from 10 to 43%. It was also revealed that samples with smaller particle crystallite sizes were found to possess more diverse adsorption sites for CO intermediate, which is important for C–C coupling of C_1 adsorbates. The group therefore asserted that, this result could offer a better platform to fully explore Cu_2O-derived Cu as ideal catalysts for producing chemical feed-stocks and fuels from CO_2 reduction.

Plasma activated Cu nanocube catalysts with tunable Cu (100) facet morphology, defect and oxygen contents was recently studied by Gao and a group of co-workers [53]. Their findings reveals a high catalytic activity and selectivity for ethylene and ethanol (Table 2). This high catalytic performance was ascribed to the presence of defects, surface and sub-surface oxygen species, including oxygen ions associated with Cu^+ species, achievable by tuning the catalysts' morphology and defect density, ion content, and surface roughness via plasma induced pre-treatment. This group therefore concluded that, the presence of oxygen species in surface and sub-surface regions of the nanocube catalysts is key for achieving high activity and hydrocarbon/alcohol selectivity, even more important than the presence of Cu(100) facets.

Oxide-derived mesoporous foam catalyst fabricated via template-assisted electrodeposition process by Dutta *et al* [54], was reported to selectively reduce CO_2 to C_2H_4 and C_2H_6 with a combined faradaic efficiency of 55% for the C_2 product as shown on Table 2. This high selectivity was attributed to due to the availability of the surface sites (i.e. surface pore diameter) for C-C coupling reaction and the temporal trapping of gaseous CO and C_2H_4 intermediates inside the mesoporous catalyst material during CO_2 electroreduction. As reported, the key point to the creation of a high abundance of surface active sites for C-C coupling for the catalyst activation was the in operando reduction of a Cu_2O phase.

In another work reported by Chung et al [55], a series of hierarchical Cu electrodes were used to catalytically convert CO_2 to formic acid and a negligible amount of CO. The peak activity was recorded for the member of the series Cu-h 5 electrode, in which it demonstrated an FE of 28% as shown in Table 2. This peak activity was due to increased (111) facet in the electrocatalyst which energetically favoured HCOOH production. This is because the majority of the surface lattice, the (111) facet, leads to the formation of Fintermediate,and as a result, CO_2 is mostly reduced to HCOOH. Another well-known intermediate is C-intermediate, which bind to the(100) facet, is presumably reduced to HCOOH. This is because enhanced electron transfer amplified by surface modification assisted the reduction to end up with HCOOH and hinders COformation.

The electrochemical reduction of CO_2 to C_2H_4 and subsequent hydrogenation to C_2H_6 was observed for a Cu_2O-derived Cu/$PdCl_2$ catalyst by Chen *et al* [56], a significant FE for ethane was observed (Table 2). Detailed mechanistic studies revealed that, CO_2 was first reduced to C_2H_4 at the Cu sites and then underwent hydrogenation with the help of the adsorbed $PdCl_x$ to generate C_2H_6. Interestingly, both sites were responsible for the reduction to C_2H_4 and subsequently to C_2H_6, but it was inferred from the study that, $PdCl_2$ dopants alongside a working electrode could offer a new methodology to expand on the type of products that could be obtained from a CO_2 building blocks.

The product yield and the relationships between surface chemistry and reaction behavior for surface oxidized copper electrodes were investigated by Keerthiga *et al* [57]. Even though there was no clear explanation for the enhanced production of ethane as the major product during electrochemical reduction of CO_2 at the surface of the electrodes, it was hypothesized that Cu (I) species played a vital role in the selectivity of the catalyst, further investigation was recommended by the group in order to understand the mechanistic details of the reaction.

However, Cu nanoclusters on single crystal (1010) ZnO electrodes were studied by Andrews and co-workers [58]. By comparing the catalytic activity/selectivity of Cu electrodes and Cu nanocluster-ZnO electrodes at a potential of -1.4V vs Ag/AgCl, it was observed that there was improved selectivity for methanol and ethanol recorded for Cu/ZnO electrode. FTIR analysis on the products obtained revealed a characteristic absorption behavior for formats and methoxy adsorbates. The mechanism for the formation of ethanol was not clear, however, the methoxy adsorbates were closely associated to alcohol since other products were obtained experimentally. Several possible mechanisms that could lead to enhanced alcohol selectivity were proposed, including reactions at Cu-Zn interfaces or charge effects arising from ZnO substrates. The ZnO may strengthen the Cu-C bond via σ-donor interactions and π back-bonding which allows for improving hydrogenation of the carbon atom, increased methoxy generation and selectivity to alcohols. However, the Cu-ZnO electrodes demonstrated a stable surface for continuous CO_2 reduction and significantly increases in alcohol yields, independent of the aforementioned pathway.

Lv *et al* [59] reported a Tin-based film on copper plate, used for the electrocatalytic reduction of carbondioxide to formate. This shows a catalytic performance with a faradaic efficiencyy of 74.1% (Table 2). This catalytic activity was influenced and enhanced by exposing the Sn/Cu electrode to air. The as-prepared Sn/Cu electrode exposed for 24 hours showed a better catalytic performance for CO_2 reduction, which was explained to be as result of the Sn film surface that became gradually oxidized and form an oxide layer which can inhibit the competing HER.

Tang *et al* [60] reported a structurally precised copper-hydride nanoclusters ($Cu_{32}H_{20}L_{12}$ where L is a dithiophosphate ligand). The major product obtained by the electrochemical synthesis on the nanocluster was $HCOO^-$ with over 80% selectivity, with other minor products such as CO and H_2 at low potentials. DFT investigation also explained that both the Cu and the hydride ligand surfaces (Fig. 5) played a vital role in pushing the reduction towards CO_2 reduction over HER at low potentials which leads to the formation of HCOOH. The HCOOH formation follows a two steps lattice-hydride reduction; CO_2 reacts directly with the capping hydride tovform HCOO* which then reacts with another interstitial hydride to form HCOOH, and then the hydride vacancies are readily regenerated by the electrochemical proton reduction.

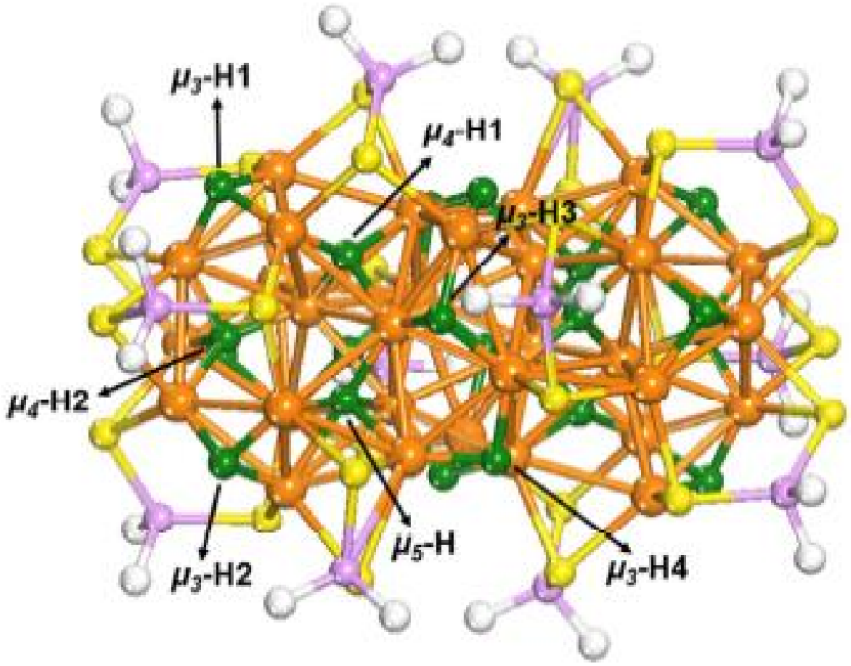

Figure 5. Atomic structure of Cu32H20L12 nanocluster (L=S2PH2). Color code: orange, Cu; green, hydride; yellow, S; purple, P; white, H on the dithiophosphate ligands. Different types of hydrides are indicated by the arrows [60].

In addition, Kim *et al* [61], have shown that by ordering the atomic transformation of AuCu nanoparticles, one could activate them as selective electrocatalyst for CO_2 reduction. Unlike the disordered alloy nanoparticles which showed preference for HER, the ordered AuCu nanoparticles selectively reduced CO_2 to CO at an FE of 80%. A structural investigation thus revealed that this enhanced catalytic activity for the ordered AuCu nanoparticles was due to the formation of a compressively strained threeatoms-thick gold overlayer that form over the inter-metallic core following the ordering transformation. This therefore suggests that surface enrichment of gold at the atomic level may be the origin of the enhanced catalytic behavior.

Concluding remarks

In this review, we have discussed the mechanistic behavior of CO_2 electrochemical reduction on various copper/copper based catalytic materials. More works should focus on utilization of porous materials and the study of the CO_2 adsorption and activation on the heterogeneous catalysts surfaces, these are very crucial for the successive reduction steps and the suppression of the competing HER. Structural and morphological controlled of eletrocatalysts should be studied extensively theoretically and experimentally. Details of how certain morphological features, and other factors that determines the selectivity of the reaction to target products were also discussed and summarized in Table 2) with the hope that this would spark up an improved interest to explore copper and copper-based materials in order to solve the world's energy and environmental challenges. However,

understanding the mechanistic aspect of CO_2 adsorption modes and effects of some operational parameter such as pH, surface functional groups, cocatalysts, and external bias needed detail attention. The mechanism of CO_2 reduction needs requires more deep investigation in the future studies. The findings of the reaction barriers and ratedetermining steps in CO_2 elctroreduction is important for the further improvement of the conversion efficiency.

Acknowledgements

Authors acknowledge the support obtained from NRF-TWAS for Doctoral Fellowship programme awarded to one of the authors (UID:105453 & Reference: SFH160618172220)

Disclosure Statement

No potential conflict of interest was reported by the authors.

Table 2. State-of-the-art progress of Cu/Cu-based electrodes

S/N	Name of Catalyst/Chemical formula (Cathode)	Morphology	Electrolyte/ p^H/physical state of the electrolyte	Overpotential	Current density	Various Products obtained	Faradaic efficiency	Anode	Cathode	Synthesis method	Reaction conditions	Ref.
1	Copper(Cu) Nanocrystals	Cu NC spheres (7.5 nm and 27 nm), Cu NC cubes (24nm, 44nm and 63 nm). Within the same morphology, smaller NCs exhibited higher activity; however, overall, the cube-shaped NCs where more intrinsically active than the spheres	CO_2-saturated 0.1M $KHCO_3$ was used as the electrolyte in aqueous medium; pH of the solution not specified	Not specified	Not specified	C_2H_4 and CH4	The selectivity of Cu NCs cubes towards CO_2RR selectivity are; 24 nm = 43% 44 nm = 80% 63 nm = 63%. FE for C_2H_4 was 41%	Platinum foil was used as the counter electrode and Ag/AgCl electrode	Cu NC Cubes /spheres spincoated on glassy carbon	For the synthesis of Cunanocubes (24, 44 and 63 nm); Varying concentration of CuBr and TOPO were dissolved into oleylamine in a threenecked flask by vigorous magnetic stirring at 80°C for 15mins. The resulting solution was heated upto 210-260°C and refluxed at this temperature for about 1-2.5h. For the synthesis of Cu spheres, 35 ml oleyamine and 3 mmol of CuBr were mixed in a three-necked flask by strong magnetic stirring at 80 °C for 15 mins, 6 mmol TOPO was injected into the mixture. After an additional stirring at 80 °C for 5 mins the mixed solution was heated upto 260 °C quickly and kept at this temperature for 3h before cooling to room temperature.	Reaction was performed at room temperature	[34]

S/N	Name of Catalyst/Chemical formula (Cathode)	Morphology	Electrolyte/ pH/physical state of the electrolyte	Overpotential	Current density	Various Products obtained	Faradaic efficiency	Anode	Cathode	Synthesis method	Reaction conditions	Ref.
										The Cubes were precipitated out by centrifugation.		
2	Copper Nanoparticle/ NDoped Graphene (Cu/CNS)	39.18nm. The CNS have a strongly curled morphology	CO_2-saturated 0.1M $KHCO_3$ electrolyte in aqueous medium. pH not specified	-1.2V vs RHE	Not specified but the maximum current density achieved at -1.0 vs RHE	C_2H_5OH, CH_4 and CO	C_2H_5OH = 63%, CH_4 = 6.8% CO = 5.2%	Glassy Carbon electrode	Cu/CNS	Not specified in the article	Reactions operated at room temperature and in water	[35]
3	Ag@Cu Bimetallic Nanoparticles	Core-shell structured Bimatallic Nanoparticles prepared at different reaction time; Ag@Cu-5, Ag@Cu-7, Ag@Cu-10, Ag@Cu-15, Ag@Cu-20 and Ag@Cu-25	Ar and CO_2saturated 0.1M $KHCO_3$ solution in aqueous medium. pH of the solution = 6.8	-1.06V vs RHE	Not specified	CO and C_2H_4	Ag@Cu-7 gave the highest FE for CO=82% and decreased dramatically to 20% for Ag@Cu-10. Ag@Cu-20 gave a peak FE for C_2H_4=28.6 %	Pt gauge and Saturated Calomel electrodes (SCE) served as counter and reference electrodes respectively	L-type glassy carbon electrode with a diameter of 5mm on which 20µL inkformulation of the electrocatalys t was dropped	The catalyst was synthesized by means of one-step polyol method to fabricate the epitaxial growth of noble metal to core-shell structure by adjusting the temperature control method and reaction time	Reactions was carried out at room temperature	[36]
4	Bimetallic Cu-Pd catalyst with different mixing pattern	Bimetallic Cu-Pd catalyst with ordered, disordered and	1M KOH electrolyte whose physical	Over potentials not specified.	The Phase separated	CO, CH_4, C_2H_4, and C_2H_5OH	Ordered CuPd=(>80 %	Not specified	Each of the Bimetallic Cu-Pd catalyst was	The reader are advised to read Ma et al 2017 [37]	The reaction	[37]

S/N	Name of Catalyst/Chemical formula (Cathode)	Morphology	Electrolyte/ p^H/physical state of the electrolyte	Overpotential	Current density	Various Products obtained	Faradaic efficiency	Anode	Cathode	Synthesis method	Reaction conditions	Ref.
		phaseseparated atomic arrangement with different atomic ratios (1:3 to 3:1).	state was not specified was used. pH was not specified.	At Cathode Potentials more positive than -0.3 vs RHE favours CO while potentials more negative than 0.3 vs RHE favours C2 products	sample achieves highest total current density of 370mA cm -3		FE for C1 products); Phaseseparated CuPd and Cu_3Pd=(>60% FE for C2 Products)		deposited onto a gas diffusion layer to form a gas diffusion Electrode (GDE)		was performed in potentiostatic mode under Ambient conditions	
5	Trace level of Cu impurities in Carbon support materials	Cu Nanoparticles electrochemically deposited on Pure Graphite (PG), Graphene Oxide (GO), and Carbon Nanotubes (CNT) all supported by Glassy Carbon (GC) and GC itself.	0.1M $NaHCO_3$ solution saturated with CO_2 for 1h pH was 6.8. To prepare Cu Spiked electrolytes, appropriate amount of Cu(ii) sulfate hydrate was added to make 0.1MNaHCO3 solutions	Overpotential was not specified but the reaction was carried out at an applied potential of 1.3V vs RHE for 2h	For Cu(2)GO/GC, the Current Density is ~4.6 $mAcm^{-3}$	H_2, CO, CH_4, and HCOOH	For both Cu(1)GO/GC and Cu(1)PG/GC, the FE for methane is about ~40%. The highest selectivity for methane is observed on	Platinum foil was used as the counter electrode while Ag/AgCl electrode was used as reference electrod.	Cu Nanoparticles drop-cast and spin-coated onto a glassy carbon	Cu Nanoparticles were synthesized by the thermal decomposition of Cu acetylacetonate ($Cu(acac)_2$) in oleylamine	Ambient pressure CO_2 electrolysis was carried out in a customary made gas-tight electrochemical cell made of polycarbonate and fitted with Buna-NO-rings	[38]
6	Cu Thin Films	Vapour Deposition of Cu Thin-film on	CO_2 purged 0.1M $KHCO_3$	CO_2 reduction was	Not specified	CH_4 , C_2H_4 and various	Not specified	Pt counter electrod	Cu thin-films on large	Thin-films of Cu were synthesized on largeformat (27mm	The experiment was	[39]

S/N	Name of Catalyst/Chemical formula (Cathode)	Morphology	Electrolyte/ p^H/physical state of the electrolyte	Overpotential	Current density	Various Products obtained	Faradaic efficiency	Anode	Cathode	Synthesis method	Reaction conditions	Ref.
		large single crystal substrates resulting in epitaxial growth in the (100), (111) and (751) out-ofplane orientations on Al_2O_3(0001), Si(100) and Si(111) substrates respectively. i.e. Cu(100), Cu(111) and Cu(751)	electrolyte whose physical state and pH were not specified	carried out within the applied potential range of 0.89V and -1-10V vs RHE		oxygenate s such as carbonyls and alcohols		e and a miniature leakless Ag/AgCl (3.4 M KCl) reference electrode	format Al_2O_3(0001), Si(100) and Si(111)	x 42mm) Al_2O_3(0001), Si(100) and Si(111) substrates in a three-source Physical Vapour Deposition (PVD).	performed using Chronoampero metry at a single potential for 1h	
7	Cu Overlayers on Tetrahexahedral Pd Nanocrystals (Cu/THH Pd NCs)	Cu Overlayers on tetrahexahedral Pd nanocrystals with (310) high-index facets	CO_2 saturated 0.1M $NaHCO_3$ (pH = 6.8). physical state of the electrolyte was not specified	-0.46 V vs RHE	Not specified	CH_3OH and C_2H_5OH	Cu_{1ML}/THH Pd NCs exhibits selectivity to C_2H_5OH at FE=~20% while Cu_{1ML}/(111)faceted Pd NCs=6.1%. CH_3OH was obatained on Cu0.8ML/THH Pd NCs with FE of 19.5%.	Pt foil, and the reference electrode was a saturated calomel electrode (SCE)	Cu_{1ML}/THH Pd NCs; Cu_{1ML}/(111)faceted Pd NCs and Cu0.8ML/THH Pd NCs. The support material not mentioned	The THH Pd NCs were prepared by a programmed square wave potential (SWP) method on a glassy carbon electrode in 0.2 mM $PdCl_2$ + 0.1 M $HClO_4$ solution. The (111)-faceted Pd NCs were prepared by constant potential electrodeposition at 0.20 V for 500 s. Cu overlayers were prepared by underpotential deposition (UPD) of Cu	The reaction was carried out under ambient conditions	[40]

S/N	Name of Catalyst/Chemical formula (Cathode)	Morphology	Electrolyte/ p^H/physical state of the electrolyte	Overpotential	Current density	Various Products obtained	Faradaic efficiency	Anode	Cathode	Synthesis method	Reaction conditions	Ref.
8	Fe-Cu Oxide Catalyst	The selective catalyst is a mixed phase material consisting of $CuFeO_2$ and CuO. Fe:Cu atomic ratio was varied from 1.3 to 0.1	0.1M CO_2 saturated H_3PO_4 buffered at pH = 7 and 0.1M $NaHCO_3$	The applied potential was −0.4 V bias vs. Ag/AgCl	Not specified	Acetate and formate	Acetate= 80% (H_3PO_4) and 76% for ($NaHCO_3$)	Pt counter electrode and Ag/AgCl as reference electrode	Fe−Cu mixed oxide, Fe_2O_3 CuO	on the Pd NCs in 1 mM $CuSO_4$ + 0.5 M H_2SO_4. The catalyst was prepared by electrodeposition on FTO glass substrate using dimethyl sulfoxide (DMSO) plating solution containing 1 mM $Cu(NO_3)_2$, 3 mM $Fe(ClO_4)_3$ and 0.1 M KClO4 electrolyte. The as-deposited catalysts was annealed at 650 °C for 3.5 hours in the air.	The reaction was carried out at −0.4 V bias vs. Ag/AgCl under constant white light illumination.	[41]
9	Cu Nanofoams	Cu Nanofoams with hierarchical porosity	0.1M $KHCO_3$, pH 6.8	The onset potential was -1.0V vs Ag/AgCl	>0.5 A/cm^2	HCOOH, H_2, and CO; C_2H_4, C_2H_6, CH_4, and C_3H_6.	FE for HCOOH was 37% at -1.5V	Copper sulfate.	Al-substrate coated with copper foam	Three-dimensional foams of copper were electrodeposited onto mechanically polished copper substrates. This procedure is simple to perform and results in an electrode with hierarchical porosity.	The reaction was performed under ambient pressure	[42]
10	Oxide-Derived Cu_xZn Catalysts	Oxide-derived Cu-based catalysts with different quantities of Zn dopants	An aqueous 0.1 M $KHCO_3$ electrolyte. pH is not specified.	The applied potential was between −0.65 and	−8.2 mA/cm^2	C_2H_5OH and C_2H_4	FE for ethanol production was 29.1% at −1.05 V vs	Ag/AgCl electrode (saturated KCl,	OxideDerived Cu_xZn	The oxide films Cu, Cu_xZn, Cu_xAg, and Cu_xNi were galvanostatically deposited onto polished Cu disks.	The reaction was performed under ambient	[43]

S/N	Name of Catalyst/Chemical formula (Cathode)	Morphology	Electrolyte/ p^H/physical state of the electrolyte	Overpotential	Current density	Various Products obtained	Faradaic efficiency	Anode	Cathode	Synthesis method	Reaction conditions	Ref.
		($Cu_{10}Zn$, Cu_4Zn, and Cu_2Zn). The asdeposited Cu oxides were in the form of smooth polyhedron particles of sizes 100 nm to 1 μm, while the Zn oxide films were interconnected platelets with lengths of hundreds of nanometers. The Cu_xZn oxide catalysts showed spherical particles that were hundreds of nanometers in sizes.		−1.15 V vs RHE			RHE,	Pine) and Pt wire were used respectively as the reference and counter electrodes.		Zinc oxide films were prepared similarly, except that they were deposited onto Zn disks. The electrodepositions were performed using a potentiostat with applied currents of −0.92 mA/cm^2 for 600 s. The electrolytes were kept at 60 °C and stirred at 300 rpm during the deposition process.	pressure in aqueous 0.1 M $KHCO_3$ electrolyte, using 60mins chronoampero metry at potentials between −0.65 and −1.15 V. The cathodic and anodic compartments of the cell were separated by an anion exchange membrane. Both compartments were infused with a continuous flow of CO_2 at 20 cm^3/min.	

S/N	Name of Catalyst/Chemical formula (Cathode)	Morphology	Electrolyte/ p^H/physical state of the electrolyte	Overpotential	Current density	Various Products obtained	Faradaic efficiency	Anode	Cathode	Synthesis method	Reaction conditions	Ref.
11	Copper(I) Oxide Catalysts	Oxide films of Cu of varying thickness	An aqueous 0.1 M $KHCO_3$ and 0.1 M K_2HPO_4 buffer was used as electrolyte was used. The latter was purified by pre-electrolysis under N_2 gas for 20h.	An overpotential of −0.99 V vs RHE was recorded. Applied potential was between −0.59 and −1.19 V vs RHE.	Not specified	C_2H_5OH and C_2H_4	34–39% for C_2H_4, and 9–16% for C_2H_5OH.	A coiled platinum wire and Ag/AgCl (Saturated KCl, Pine) served as counter and reference electrodes, respectively.	Copper(I) Oxide	Flat Cu discs, served as substrates for all the catalysts. They were first polished to a mirror-like finish using SiC paper and diamond slurries. Cu_2O layers were then galvanostatically deposited onto these Cu discs from a copper lactate solution. Cu_2O films of different thicknesses were obtained by varying the deposition time between 1 and 60 min. Seven Cu_2O films with varying thicknesses were prepared. Electropolished Cu surfaces were prepared by electropolishing the copper discs at +260 mA/cm2 for 60 s in 85% phosphoric acid, followed by rinsing with ultrapure water.	A custom-built, gastight Teflon electrochemical cell. The cathodic and anodic compartments, separated by an anionexchange membrane, were filled with 10 and 8 cm^3 of electrolyte separately. The volume of the headspace in the cathodic compartment was 2 cm^3.	[44]
12	Nanodendritic Cu catalyst	In situ deposited copper nanodendrites	0.1 M KBr was used as catholyte	The optimized working	170 mA cm^{-2}.	C_2H_4	57%	A solid IrOx coated	Cu nanodendrites	Cu nanodendrites were obtained during an in situ	The CO_2 reduction was	[45]

S/N	Name of Catalyst/Chemical formula (Cathode)	Morphology	Electrolyte/ p^H/physical state of the electrolyte	Overpotential	Current density	Various Products obtained	Faradaic efficiency	Anode	Cathode	Synthesis method	Reaction conditions	Ref.
			(100 mL) and 1 M $KHCO_3$ as anolyte (100 mL). p^H was not specified.	potential of the cathode was located in a voltage range experiments between (−1.5 and −1.55 V) versus Ag/AgCl.				Ti electrode was used as counter electrode.		electro deposition in acidic medium (pH = 2.5) under high over potential (<-2 V vs Ag/AgCl).	carried out under constant current (170 mA cm^{-2}) to maintain stable electrolysis conditions. The electrolyte flow was controlled by an eight channel peristaltic pump at a flow rate of 100 mL min^{-1}.	
13	Cu/SnO_2 Core/Shell Structure	A thin layer of SnO_2, coated over Cu nanoparticles, with a Cu/SnO_2 core/shell nanoparticle structure.	CO_2 saturated 0.5 M $KHCO_3$ was used as the electrolyte. The p^H of the electrolyte was not mentioned.	The onset potential of CO_2 reduction to CO is at -0.5 V, while the highest FE was achieved at a potential of 0.7 V vs RHE.	4.6 mA/cm^2	CO, H_2 and formate.	FE for Co was recorded as 93%. When the SnO_2 shell becomes thicker (1.8 nm), the core/shell NPs function as a SnO_2 NP	The counter/reference electrodes were not mentioned in the main text	core/shell Cu/SnO_2 NPs	Monodisperse core/shell Cu/SnO_2 NPs were synthesized via a seedmediated method via the decomposition of tin acetylacetonate ($Sn(acac)_2$) in the presence of 7 nm Cu NPs at 250°C for 1 h. in this synthesis, the SnO_2 shell thickness was	The reaction was performed at ambient conditions of pressure and temperature.	[46]

S/N	Name of Catalyst/Chemical formula (Cathode)	Morphology	Electrolyte/ p^H/physical state of the electrolyte	Overpotential	Current density	Various Products obtained	Faradaic efficiency	Anode	Cathode	Synthesis method	Reaction conditions	Ref.
							catalyst and formate is the major product (85% FE at 0.9 V)			controlled by the amount of $Sn(acac)_2$ added.		
14	Copper Oxide catalyst	Electrodeposited cuprous oxide thin film	An aqueous 0.5M $KHCO_3$ saturated with ultrapure CO_2 was used as electrolyte. P^H of 7.6	The reaction was conducted at potentials ranging from −1.0 to −1.9 V (SCE).	Current density was not recorded in the main text	CH_3OH, H_2, and trace amounts of CO.	38% for CH_3OH	Ag/AgCl electrode saturated with NaCl was selected as the reference electrode along with a Pt wire as the counter electrode.	Cuprous oxide thin Films, electrodeposited on stainless steel substrates was used as the cathode	Electrodes for CO2 reduction were fabricated via oxidization of Cu foils or thin film electrodeposition. Airoxidized electrodes were prepared by first cleaning the foil in 0.1 M HCl for 20 s followed by oxidation in an air furnace at 403 K for 17 h. Anodized electrodes were created by electrochemically oxidizing Cu foil in 0.5 M $KHCO_3$ at a constant potential of 1.25 V (SCE) for 3 min. Cuprous oxide thin films were electrodeposited on stainless steel substrates at − 0.555 V (SCE) and 333 K for 30 min in a lactate	CO_2 reduction experiments were performed in a typical three electrode cell (30 mL volume). During the reaction, CO_2 was bubbled into the electrolyte for 30mins at 298K.	[47]

S/N	Name of Catalyst/Chemical formula (Cathode)	Morphology	Electrolyte/ p^H/physical state of the electrolyte	Overpotential	Current density	Various Products obtained	Faradaic efficiency	Anode	Cathode	Synthesis method	Reaction conditions	Ref.
15	CuO derived Copper catalysts	CuO-derived porous copper nanoribbon arrays	Co_2 gas bubbled in aqueous 0.1M $KHCO_3$ solution via gas dispenser was used as the electrolyte. P^H was not mentioned.	The overpotential recorded was −0.816 V vs. RHE	Current density was not recorded in the main text	The products obtained are C_2H_4, $C_2H_6$and C_2H_5OH	The total FE for the C_2 compounds is ~40%	A Pt foil and Ag/AgCl were used as the counter and reference electrode, respectively.	CuO derived Copper	solution including 0.4 M CuSO4 and 3 M lactic acid at pH 9.0 with Cu foil as the anode. CuO-derived porous Cu NRAs electrode was prepared by the electrochemical reduction of CuO NRAs. NaOH, NaCl , $Na_2S_2O_8$, and $CuSO_4$ were dissolved into 100 mL deionized water. Cu foil with a geometric surface area of 4 cm^2 was immersed in the as-prepared solution at 86°C for 8 min, during which Cu was oxidized to CuO. The foil was then taken out of the solution, rinsed with deionized water, and dried in air. A thin layer of Cu_2O was grown in a basic solution, which included NaOH, NaCl, and $CuSO_4$, at temperature of 60°C for 10 s. The CuO NRA electrode was reduced under −0.18 V vs. RHE for 30 min to obtain Cu	The reaction was conducted under ambient pressure and temperature. The potentiostatic electrolysis of CO2 was carried out in a conventional three-electrode cell by using a potentiostat	[48]

S/N	Name of Catalyst/Chemical formula (Cathode)	Morphology	Electrolyte/ p^H/physical state of the electrolyte	Overpotential	Current density	Various Products obtained	Faradaic efficiency	Anode	Cathode	Synthesis method	Reaction conditions	Ref.
										electrodes consisting of nanoporous ribbon array structure.		
16	Cu_2O-derived copper nanoparticles	Cuprous oxide films with [100], [110] and [111] orientation and variable thickness	85 ml of 0.1 M $KHCO_3$ was used as electrolyte at pH 6.8, as obtained after saturation with CO_2. CO_2 was continuously purged at a rate of 20 ml min^{-1} for 30 minutes before each experiment, to attain saturation of the electrolyte. Then the flow rate was decreased to 5 ml min^{-1}.	The electrochemical reduction at a cathodic potential of 1.1 V vs RHE	0.8 mA cm^{-2} at pH 12 favours triangular pyramid orientation in the (110) direction where the (100) and (010) facets are exposed. Increasing the current density to 2 mA cm^{-2} at pH 12 favours the growth in (100)	CO, methane, ethylene ethane and ethylene	Not specified	Pt mesh was used as a counter electrode and Ag/AgCl was used as reference electrode.	Cu_2O-derived copper nanoparticles	Cuprous oxide films with [100], [110] and [111] orientation and variable thickness were electrodeposited by reduction of copper(II) lactate on commercially available copper plates from Cu_2^+ containing solutions prepared using 0.4 M $CuSO_4$ and 3 or 4 M lactic acid at 60 or 70°C. The electrodeposition was conducted in a standard three-electrode cell where platinum mesh and Ag/AgCl in 3 M NaCl served as counter and reference electrodes, respectively.	Electrochemical CO_2 reduction was carried out in a glass cell using a three electrode assembly at room temperature and pressure.	[49]

S/N	Name of Catalyst/Chemical formula (Cathode)	Morphology	Electrolyte/ p^H/physical state of the electrolyte	Overpotential	Current density	Various Products obtained	Faradaic efficiency	Anode	Cathode	Synthesis method	Reaction conditions	Ref.
					directions with threefaced pyramids, where the sides of the pyramids expose (111) facets.							
17	Copper NPs and reduced graphene oxide nanocomposite catalyst (Cu-rGO)	Unique nanocomposite consisting of Cu nanoparticles (NPs) and reduced graphene oxide (rGO) supported on a Cu substrate. The nanocomposite was optimized in terms of the composition of Cu NPs and rGO as well as the overall amount.	The electrolyte used was CO2 saturated 0.1M $NaHCO_3$ solution whose pH was 6.65.	The overpotential recorded was −0.4 V (vs. RHE)	Not specified	CO, HCOOH and CH_4.	76.6%	Ar-saturated 0.1 M $NaHCO_3$ and Arsaturated 0.1 M Na2SO4 whereas, the reference electrode used was Ag/AgCl	Nanocomposite consisting of Cu nanoparticles (NPs) and reduced graphene oxide (rGO) supported on a Cu substrate was used as the cathode	The Cu-rGO nanocomposite was formed directly on a Cu substrate using a facile electrochemical reduction method. A mixture of GO and Cu_2^+ precursors was cast on an etched Cu substrate; and the simultaneous formation of Cu-rGO nanocomposite was achieved via cyclic voltammetry (CV), which was carried out in 0.1 M Na2SO4 in the potential range from 0.62 to −0.58 V vs. RHE for five cycles. The composition	The reaction was conducted at three potentials (−0.4, −0.5, and −0.6 V) for six hours of electrolysis. A gas-tight twocompartment electrochemical cell was used for the product formation and analy	[50]

S/N	Name of Catalyst/Chemical formula (Cathode)	Morphology	Electrolyte/ p^H/physical state of the electrolyte	Overpotential	Current density	Various Products obtained	Faradaic efficiency	Anode	Cathode	Synthesis method	Reaction conditions	Ref.
										and thickness of the formed Cu-rGO nanocomposite were also optimized	sis. A cationic exchange membrane was utilized as a separator in the cell. Each compartment contained 35.0 ml of the electrolyte	
18	Nanoporous copper films catalysts	Nano Porous Copper Films by AdditiveControlled Electrodeposition. The morphologies of the Cu films are varied to exhibit wire, dot, or amorphous structures.	the electrolyte used was CO_2 saturated $KHCO_3$ aqueous solution. pH was not specified	The cathodic potentials recorded are -0.5 V vs. RHE for C_2H_4 and 0.5 V vs. RHE for C_2H_5OH	Not s	C_2H_4, and C_2H_5OH	The FE recorded are 40% for C_2H_4 and 20% for C_2H_5OH	Pt mesh counter electrode and an Ag/AgCl reference electrode were used. The Ag/AgCl reference electrode was calibrat	Nanoporous copper films catalysts	Nanoporous Cu film from plating baths containing 3,5-diamino-1,2,4-triazole (DAT) as an inhibitor was synthesized using electrodeposition method with high surface area and tunable morphology.	Cyclic voltammetry (CV), chronoampero metry (CA), and chronopotentiometry (CP) evaluating CO_2 reduction performed room temperature.	[51]

S/N	Name of Catalyst/Chemical formula (Cathode)	Morphology	Electrolyte/ p^H/physical state of the electrolyte	Overpotential	Current density	Various Products obtained	Faradaic efficiency	Anode	Cathode	Synthesis method	Reaction conditions	Ref.
								ed before each experiment with a normal hydrogen electrode (NHE) in 1M $HClO_4$.				
19	Cu_2O-Derived Copper Catalysts	Cu films of different thicknesses and morphologies	Aqueous 0.1 M $KHCO_3$ was used as the electrolyte. pH of 6.8.	Electrochemistry and quantification of the products was measured at the potential of -0.98V vs RHE	−31.2 mA cm^{-2}.	C_2H_4, ethanol and npropanol	FEs of 42.6% (jC_2H_4 = −13.3 mA cm^{-2}), 11.8% (jC_2H_5OH = −3.7 mA cm^{-2}), and 5.4% ($jC_3H{=}OH$ = −1.7 mA cm^{-2}), were recorded respectively.	Ag/AgCl and Pt wire are used as the reference and counter electrodes respectively	Cu_2ODerived Copper Catalysts	Cu_2O films were grown hydrothermally onto mechanically polished Cu discs suspended on a custom-made Teflon holder in a Teflon-lined stainless steel autoclave at 145 °C for 90 min. A precursor solution consisting of 0.25 M of $Cu(NO_3)_2{\cdot}3H_2O$ and 0−1.75 M NH_3 dissolved in a solvent was used. The solvent consisted of a 23:13:2 volumetric ratio of ethanol, ultrapure water, formic and acid . The thickness of the films	Electrochemical measurements were performed using a Gamry 600 galvanostat/potentiostat using a threeelectrode configuration. The electrodes were housed in a custommade,	[52]

S/N	Name of Catalyst/Chemical formula (Cathode)	Morphology	Electrolyte/ p^H/physical state of the electrolyte	Overpotential	Current density	Various Products obtained	Faradaic efficiency	Anode	Cathode	Synthesis method	Reaction conditions	Ref.
										was expected to increase with the concentration of the NH_3. The as-prepared Cu2O films were then washed with copious amounts of water, dried overnight at 60 °C and prereduced to Cu0 in a separate 0.1 M $KHCO_3$ electrolyte for 300 s, before being used as catalysts for CO_2 reduction. We termed these as Cu_2O-derived Cu.	gastight, two compartment Teflon cell.	
20	Plasma-Activated Copper Nanocube Catalysts	Cu nanocube catalysts with tunable Cu(100) facet	CO_2-saturated 0.1 M $KHCO_3$ solution (pH 6.8) was used as the electrolyte in aqueous medium.	The applied potential recorded was −1.0 V *vs* RHE for 1 h.	Not specified	C_2 and C_3	Maximum FE for C_2 and C_3 is ~73%	Pt gauze and leakfree Ag/AgCl were used as counter and reference electrodes respectively	Activated Copper Nanocube Catalysts	Commercial Cu foils were first cleaned with acetone and ultra-pure water in an ultrasonic bath, and then electropolished in phosphoric acid at 3 V vs titanium foil for 5 min. Cu nanocubes were prepared by electrochemically anodizing the electropolished Cu foils in 0.1 M KCl with five triangular potential scans ranging from	Electrochemical measurements were carried out in a gastight H-cell separated by a Nafion 115 membrane.	[53]

S/N	Name of Catalyst/Chemical formula (Cathode)	Morphology	Electrolyte/ p^H/physical state of the electrolyte	Overpotential	Current density	Various Products obtained	Faradaic efficiency	Anode	Cathode	Synthesis method	Reaction conditions	Ref.
										0.4 V to 2.0 V vs RHE at a rate of 500 mV s−1. During each cycle, the potential was held at the positive and negative limits for 10 and 5 seconds, respectively. The Cu nanocube samples were then rinsed with a large amount of ultra-pure water to remove the electrolyte. Plasma pre-treatments were then performed in a plasma etcher at a gas pressure of 400 mTorr of O2, H2 or Ar and power of 20 W for different periods of time.		
21	Oxide-derived Cu foam catalysts	Mesoporous Cu foams	CO_2 saturated 0.5M $NaHCO_3$ in aqueous medium. pH not mentioned	between -0.4 to -1.0 vs RHE.	Highest at -1.0 V and are in the order of 57 mA/cm^2	H_2, CO, $HCOO^-$, CH_4, C_2H_4 and C_2H_6	C_2 efficiencies reaching FEC_2 = 55%. The total FE of all the major products lies between 89% and 96%.	A leakless Ag/$AgCl_{3M}$ He Was used as treference electrode and a bright Pt-foil (15mm x 5mm)	Cu foam catalysts.	Mesoporous Cu foam catalysts were electrodeposited on Cu blanket wafer coupons by a through mask plating process leaving a welldefined area covered with the Cu foam behind.	The electrolysis was carried out in a custom-built, air-tight glass cell (H-type).	[54]

S/N	Name of Catalyst/Chemical formula (Cathode)	Morphology	Electrolyte/ p^H/physical state of the electrolyte	Overpotential	Current density	Various Products obtained	Faradaic efficiency	Anode	Cathode	Synthesis method	Reaction conditions	Ref.
22	Hierarchical Cu pillar electrode catalyst	Highly perpendicular Cu pillar Structures	The electrolyte used was CO_2bubbled 0.1 M $KHCO_3$ aqueous solution (pH 6.66.7).	The electrochemical conversion of CO_2 at various constant potentials (i.e. from −0.2 to −0.9 V vs. RHE). Recorded overpotential formic acid was −0.5 V (vs. RHE).	Not specified	formic acid, HCOOH.	The Cu-5 h electrode performed well with a 28 % FE to formic acid.	was used as counter electrode The standard calomel electrode (SCE) and Pt gauze were used as the reference and counter electrodesrespectively.	Hierarchical Cu pillar structureswer e used as the working electrode	Cu pillar electrodes (Cu2.5 h, Cu-5 h) was fabricated by using an electrodeposition method i.e. Highly perpendicular Cu nanopillar structure was prepared by cathodic electrodeposition on a Cu foil substrate	Electrolyses were performed on a fuel-cell-like twocompartment electrochemical cell separated by a piece of selemion anion exchange membrane.	[55]
23	Nanostructured Cu_2ODerived Cu Catalyst /Palladium(II) Chloride	Cu_2O nanoparticles deposited on polished Cu disc electrode. The surface of an electropolished Cu electrode was smooth and featureless	The electrolyte used was aqueous 0.1 M $KHCO_3$ + 100mg $PdCl_2$. pH 6.8.	The conversion was performed at −1.0 V vs RHE	Not specified	C2 products i.e. C_2H_4, C_2H_6 and ethanol.	FE of 3.4% was recorded for C_2H_4, and FE of 30.1% for C_2H_6.	The counter and reference electrodes were a Pt wire and a Ag/AgCl electrode	The working electrode was Cu_2O nanoparticles deposited on polished Cu disc electrode	Cu_2O was electrochemically deposited onto a polished Cu electrode using a twoelectrode cell with a platinum counter electrode. Deposition was performed at 60 °C, with a fixed current of −0.7 mA for 1200 s.	The electrochemical reduction of CO_2 was performed in a Gas tight Teflon electrochemical cell.	[56]

S/N	Name of Catalyst/Chemical formula (Cathode)	Morphology	Electrolyte/ p^H/physical state of the electrolyte	Overpotential	Current density	Various Products obtained	Faradaic efficiency	Anode	Cathode	Synthesis method	Reaction conditions	Ref.
								(Saturated KCl, Pine Research Instrumentation), respectively.				
24	Surface Oxidized Copper Catalyst	Pure Cu metal sheet 4cm^3, modified by surface oxidation.	The lectrolyte used was CO_2 saturated 0.5 Mdm^{-3} KCl.	The conversion was performed within the range of -0.9 to -2 V vs Ag/AgCl	Not specified	Methane and ethane	Not specified	Ag/AgCl saturated KCl was used as reference electrode and Pt foil as counter electrode	The working electrode was Surface Oxidized Copper Electrodes	The metal electrodes used in the present study are pure Cu sheet of 4 cm2 where electrical connection is established through the same strip. The Cu strips were polished with fine emery paper and electrolytically treated in 1 mol dm-3 phosphoric acid and sulphuric acid, cleaned with acetone to remove grease, washed subsequently with water and used as working electrode. The same Cu electrodes were modified by exposing them to high temperature oxygen	The electrochemical measurements were conducted with an EC epsilon potentiostat. The experiments were performed in a laboratorymade H-cell	[57]

S/N	Name of Catalyst/Chemical formula (Cathode)	Morphology	Electrolyte/ p^H/physical state of the electrolyte	Overpotential	Current density	Various Products obtained	Faradaic efficiency	Anode	Cathode	Synthesis method	Reaction conditions	Ref.
										mixed LPG gas at a flame temperature of 900 ºC, referring as surface oxidized Cu electrode.		
25	Cu Nanoclusters	Cu nanoclusters on single crystal (1010) ZnO electrodes.	Electrochemical experiments were carried out in aqueous 0.1 M $KHCO_3$ electrolytes saturated with CO_2	The reduction experiments was conducted at −1.4 V versus Ag/AgCl	Not specified	H_2, C_2H_5OH, C_2H_4, $HCOO^-$, CO, CH_3OH, and CH_4.	H_2 (45.1%), C_2H_5OH (10.2%), C_2H_4 (10.1%), $HCOO^-$ (7.7%), CO (5.4%), CH_3OH (2.8%), CH_4 (1.8).	Ag/AgCl (saturated with NaCl) was used as reference electrode and Pt. as counter electrode.	The working electrode was single crystal cathode (With Cu nanoclusters).	Electrodes were fabricated by cleaning single crystal ZnO (1010) substrates, followed by vacuum deposition of Cu.	Electrochemic al experiment was conducted in a single compartment PTFE cell	[58]
26	Tin Based Film on Copper Plate.	Sn/Cu electrode with the geometric surface area of $1cm^2$	The electrolyte used was 40 mL of 0.1 mol L^{-1} $KHCO_3$ aqueous solution, saturated with CO_2. pH not specified in the text	The electrolysis was carried out at a potential of −1.8 V vs. Ag/AgCl	5.08 mA cm^{-2}.	Formate	74.1% at −1.8 V.	Pt plate and an Ag/AgCl electrode (sat. KCl) were used as counter and reference electrodes respectively.	The working electrode was Sn based film on Cu electrode (i.e. prepared Sn/Cu electrode with the geometric surface area of 1 cm^2.	Sn based film with a thickness of 169 nm was electrodeposited on copper plate from a choline chloride/ethylene glycol based electrolyte containing $SnCl_2$. The electrochemical deposition was performed on the Cu substrate in nonaqueous solution containing 0.1 mol L^{-1} $SnCl_2$.	Electrolysis was carried out potentiostatically using a LAND CT2001C cell performancetesting instrument	[59]

S/N	Name of Catalyst/Chemical formula (Cathode)	Morphology	Electrolyte/ pH/physical state of the electrolyte	Overpotential	Current density	Various Products obtained	Faradaic efficiency	Anode	Cathode	Synthesis method	Reaction conditions	Ref.
27	Copper-Hydride Nanoclusters	Structurally precise ligand protected Cu-hydride nanoclusters, such as $Cu_{32}H_{20}L_{12}$ (L is a dithiophosphate ligand). i.e. composite Cu32/C/GDL electrode	The electrolytes used are 60 mL of 0.1 M KHCO3 and 0.4 M KCl solution saturated with CO_2. pH of 6.8	The onset potentials for the conversion of CO_2 to HCCOH and CO are -0.32 V and -0.81 V vs. SHE, respectively. The over potential recorded are (0.3V, 0.4V) and (0.5V, 0.6V) for the production of HCOOH and H2 respectively.	Not specified	HCOOH, H_2 and CO.	Cumulative FE for the 3 products is >90%. Cu32H20L12 nanocluster predominantly produces HCOOH at low overpotentials (89% at 0.3 V and 83% at 0.4 V). By contrast, the product selectivity dramatically changes when the overpotential is higher than 0.5 V where H2 is predominantly produced (85% at 0.5 V and 94% at 0.6 V).	Pt. plate (1.68 cm^2) and Ag/AgCl (3 M NaCl) are used as counter and reference electrodes respectively.	The working electrode was a composite made from the Nanoclusters, carbon black and gas diffusion layer electrode	Synthesis method for the Nanoclusters was not specified in the main text. However, The composite working electrode was fabricated by spreading a catalyst ink, prepared by mixing 80 µg of the $Cu_{32}(H)_{20}\{S_2P(OiPr)_2\}_{12}$ cluster catalyst, 200 µg of carbon black and 3.5 µL of Nafion solution in 50 µL of tetrahydrofuran, on a gas diffusion layer electrode (2 cm2).	Controlled potential electrolysis (CPE) experiments were Carried out for 90 min under vigorous stirring with a ZIVE MP1 potentiostat in an H-type cell. The working electrode and the counter electrode were separated by a protone xchange membrane	[60]

S/N	Name of Catalyst/Chemical formula (Cathode)	Morphology	Electrolyte/ p^H/physical state of the electrolyte	Overpotential	Current density	Various Products obtained	Faradaic efficiency	Anode	Cathode	Synthesis method	Reaction conditions	Ref.
28	AuCu Nanoparticles	Atomic Ordering Transformations of AuCu Nanoparticles. E.g. *d*-AuCu and *o*AuCu NPs.	The measurements was conducted at −0.77 V vs RHE	0.43 mA/cm^2 for *d*-AuCu NP to 1.39 mA/cm^2 for *o*-AuCu NP		CO	80%	Pt. wire was used as a counter electrode and Ag/AgCl (3 M KCl) as a reference electrode.	The working electrode was 4 µg of each AuCu NP drop-casted onto a carbon paper electrode	Au seed nanoparticles were fisrt synthesized. The as-synthesized Au NPs (0.25 mmol) were dispersed in 20 mL of hexane and used as seeds for AuCu NP synthesis. A typical synthesis procedure was carried out in a Schlenk line.	The reduction was conducted at standard electrochemical conditions at 1atm CO_2 and room temperature.	[61]

References

[1]. Dresselhaus M.S., Thomas I.L. *Nature*, 2001, **414**:332 [Crossref], [Google Scholar], [Publisher]
[2]. Chu S., Majumdar A. *Nature*, 2012, **488**:294 [Crossref], [Google Scholar], [Publisher]
[3]. Canadell J.G., Le Quéré C., Raupach M.R., Field C.B., Buitenhuis E.T., Ciais P., Conway T.J., Gillett N.P., Houghton R.A., Marland G. *Proc. Natl. Acad. Sci.*, 2007, **104**:18866 [Crossref], [Google Scholar], [Publisher]
[4]. Tans P., Keeling R. *URL Http//Www. Esrl. Noaa.* 14. *Gov/Gmd/Ccgg/Trends*. 2013 [Google Scholar], [Publisher]
[5]. Feldman D.R., Collins W.D., Gero P.J., Torn M.S., Mlawer E.J., Shippert T.R. *Nature*, 2015, **519**:339 [Crossref], [Google Scholar], [Publisher]
[6]. Mann M.E. *Proc. Natl. Acad. Sci.*, pnas-0901303106, 2009 [Crossref], [Google Scholar], [Publisher]
[7]. Larcher D., Tarascon J.M. *Nat. Chem.*, 2015, **7**:19 [Crossref], [Google Scholar], [Publisher]
[8]. Figueroa J.D., Fout T., Plasynski S., McIlvried H., Srivastava R.D. *Int. J. Greenh. Gas Control*, 2008, **2**:9 [Crossref], [Google Scholar], [Publisher]
[9]. Olajire A.A. *Energy*, 2010, **35**:2610. [Crossref], [Google Scholar], [Publisher]
[10]. MacDowell N., Florin N., Buchard A., Hallett J., Galindo A., Jackson G., Adjiman C.S., Williams C.K., Shah N., Fennell P. *Energy Environ. Sci.*, 2010, **3**:1645 [Crossref], [Google Scholar], [Publisher]
[11]. Kondratenko E.V., Mul G., Baltrusaitis J., Larrazábal G.O., Pérez-Ramírez J. *Energy Environ. Sci.*, 2013, **6**:3112 [Crossref], [Google Scholar], [Publisher]
[12]. Spinner N.S., Vega J.A., Mustain W.E. *Catal. Sci. Technol.*, 2012, 2:19 [Crossref], [Google Scholar], [Publisher]
[13]. Whipple D.T., Kenis P.J.A. *J. Phys. Chem. Lett.*, 2010, 1:3451 [Crossref], [Google Scholar], [Publisher]
[14]. Hori Y., *Electrochemical CO 2 reduction on metal electrodes;* Springer: New York, 2008; p 89 [Crossref], [Google Scholar], [Publisher]
[15]. Jitaru M., Lowy D.A., Toma M., Toma B.C., Oniciu L. *J. Appl. Electrochem.*, 1997, **27**:875 [Crossref], [Google Scholar], [Publisher]
[16]. Sanchez-Sanchez C.M., Montiel V., Tryk D.A., Aldaz A., Fujishima A. *Pure Appl. Chem.*, 2001, **73**:1917 [Crossref], [Google Scholar], [Publisher]
[17]. Chen C.S., Handoko A.D., Wan J.H., Ma L., Ren D., Yeo B.S. *Catal. Sci. Technol.*, 2015, **5**:161 [Crossref], [Google Scholar], [Publisher]
[18]. Zhu W., Michalsky R., Metin Ö., Lv H., Guo S., Wright C.J., Sun X., Peterson A.A., Sun S., *J. Am. Chem. Soc.*, 2013, **135**:16833 [Crossref], [Google Scholar], [Publisher]
[19]. Zhang S., Kang P., Ubnoske S., Brennaman M.K., Song N., House R.L., Glass J.T., Meyer T.J., *J. Am. Chem. Soc.*, 2014, **136**:7845 [Crossref], [Google Scholar], [Publisher]
[20]. Hoshi N., Kato M., Hori Y., *J. Electroanal. Chem.*, 1997, **440**:283 [Crossref], [Google Scholar], [Publisher]
[21]. Hori Y., Wakebe H., Tsukamoto T., Koga O., *Electrochim. Acta*, 1994, **39**:1833 [Crossref], [Google Scholar], [Publisher]
[22]. DiMeglio J.L., Rosenthal J., *J. Am. Chem. Soc.*, 2013, **135**:8798 [Crossref], [Google Scholar], [Publisher]
[23]. Ding C., Li A., Lu S.-M., Zhang H., Li C. *ACS Catal.*, 2016, **6**:6438 [Crossref], [Google Scholar], [Publisher]
[24]. Lee C.H., Kanan M.W. *ACS Catal.*, 2014, 5:465. [Crossref], [Google Scholar], [Publisher]
[25]. Won D.H., Shin H., Koh J., Chung J., Lee H.S., Kim H., Woo S.I. *Angew. Chemie Int. Ed.*,

2016, **55**:9297 [Crossref], [Google Scholar], [Publisher]
[26]. Varela A.S., Ranjbar Sahraie N., Steinberg J. , Ju W., Oh H., Strasser P. *Angew. Chemie Int. Ed.*, 2015, **54**:10758 [Crossref], [Google Scholar], [Publisher]
[27]. Liu Y., Chen S., Quan X., Yu H. *J. Am. Chem. Soc.*, 2015, **137**:11631 [Crossref], [Google Scholar], [Publisher]
[28]. Kuhl K.P., Cave E.R., Abram D.N., Jaramillo T.F. *Energy Environ. Sci.*, 2012, **5**:7050 [Crossref], [Google Scholar], [Publisher]
[29]. Lim R.J., Xie M., Sk M.A., Lee J.-M., Fisher A., Wang X., Lim K.H. *Catal. Today*, 2014, **233**:169 [Crossref], [Google Scholar], [Publisher]
[30]. Schlögl R. *Angew. Chemie Int. Ed.*, 2015, **54**:3465 [Crossref], [Google Scholar], [Publisher]
[31]. Qiao J., Liu Y., Hong F., Zhang J. *Chem. Soc. Rev.*, 2014, **43**:631 [Crossref], [Google Scholar], [Publisher]
[32]. Albo J., Alvarez-Guerra M., Castaño P., and Irabien A. *Green Chem.*, 2015, **17**:2304 [Crossref], [Google Scholar], [Publisher]
[33]. Vickers J.W., Alfonso D., Kauffman D.R. *Energy Technol.*, 2017, **5**:775 [Crossref], [Google Scholar], [Publisher]
[34]. Loiudice A., Lobaccaro P., Kamali E.A., Thao T., Huang B.H., Ager J.W., Buonsanti R., *Angew. Chemie Int. Ed.*, 2016, **55**:5789 [Crossref], [Google Scholar], [Publisher]
[35]. Song Y., Peng R., Hensley D.K., Bonnesen P. V, Liang L., Wu Z., Meyer H.M., Chi M., Ma C., Sumpter B.G., *ChemistrySelect*, 2016, **1**:6055 [Crossref], [Google Scholar], [Publisher]
[36]. Chang Z., Huo S., Zhang W., Fang J., Wang H. *J. Phys. Chem. C*, 2017, **121**:11368 [Crossref], [Google Scholar], [Publisher]
[37]. Ma S., Sadakiyo M., Heima M., Luo R., Haasch R.T., Gold J.I., Yamauchi M., Kenis P.J.A., *J. Am. Chem. Soc.*, 2016, **139**:47 [Crossref], [Google Scholar], [Publisher]
[38]. Lum Y., Kwon Y., Lobaccaro P., Chen L., Clark E.L., Bell A.T., Ager J.W. *ACS Catal.*, 2015, **6**:202 [Crossref], [Google Scholar], [Publisher]
[39]. Hahn C., Hatsukade T., Kim Y.G., Vailionis A., Baricuatro J.H., Higgins D.C., Nitopi S.A., Soriaga M.P., Jaramillo T.F. *Proc. Natl. Acad. Sci.*, 2017, **114**:5918 [Crossref], [Google Scholar], [Publisher]
[40]. Zhang F.Y., Sheng T., Tian N., Liu L., Xiao C., Lu B.A., Xu B.B., Zhou Z.Y., Sun S.G. *Chem. Commun.*, 2017, **53**:8085 [Crossref], [Google Scholar], [Publisher]
[41]. Yang X., Fugate E.A., Mueanngern Y., Baker L.R. *ACS Catal.*, 2016, **7**:177 [Crossref], [Google Scholar], [Publisher]
[42]. Sen S., Liu D., Palmore G.T.R., *Acs Catal.*, 2014, **4**:3091 .[Crossref], [Google Scholar], [Publisher]
[43]. Ren D., Ang B.S.H., Yeo B.S. *Acs Catal.*, 2016, **6**:8239 [Crossref], [Google Scholar], [Publisher]
[44]. Ren D., Deng Y., Handoko A.D., Chen C.S., Malkhandi S., Yeo B.S. *ACS Catal.*, 2015, **5**:2814 [Crossref], [Google Scholar], [Publisher]
[45]. Reller C., Krause R., Volkova E., Schmid B., Neubauer S., Rucki A., Schuster M., Schmid G. *Adv. Energy Mater.*, 2017, **7**:1602114 [Crossref], [Google Scholar], [Publisher]
[46]. Li Q., Fu J., Zhu W., Chen Z., Shen B., Wu L. , Wang T., Lu G., Zhu J. *J. Am. Chem. Soc.*, 2017, **139**:4290 [Crossref], [Google Scholar], [Publisher]
[47]. Le M., Ren M., Zhang Z., Sprunger P.T., Kurtz R.L., Flake J.C. *J. Electrochem. Soc.*, 2011, **158**:E45 [Crossref], [Google Scholar], [Publisher]
[48]. Ke F.S., Liu X.C., Wu J., Sharma P.P., Zhou Z.Y., Qiao J., Zhou X.D. *Catal. Today*, 2017, **288**:18 [Crossref], [Google Scholar], [Publisher]
[49]. R. Kas, R. Kortlever, A. Milbrat, M.T.M. Koper, G. Mul, J. Baltrusaitis, *Phys. Chem. Chem. Phys.*, 2014, **16**:12194. [Crossref], [Google Scholar], [Publisher]

[50]. Hossain M.N., Wen J., Chen A., *Sci. Rep*., 2017, **7**:3184 [Crossref], [Google Scholar], [Publisher]
[51]. Hoang T.T.H., Ma S., Gold J.I., Kenis P.J.A., Gewirth A.A. *ACS Catal*., 2017, **7**:3313 [Crossref], [Google Scholar], [Publisher]
[52]. Handoko A.D., Ong C.W., Huang Y., Lee Z.G., Lin L., Panetti G.B., Yeo B.S. *J. Phys. Chem. C*, 2016, **120**:20058 [Crossref], [Google Scholar], [Publisher]
[53]. Gao D., Zegkinoglou I., Divins N.J., Scholten F., Sinev I., Grosse P., Roldan Cuenya B. *ACS Nano*, 2017, **11**:4825 [Crossref], [Google Scholar], [Publisher]
[54]. Dutta A., Rahaman M., Luedi N.C., Mohos M., Broekmann P., *ACS Catal*., 2016, **6**:3804 [Crossref], [Google Scholar], [Publisher]
[55]. Chung J., Koh J., Kim E.H., Woo S.I. , Phys. Chem. Chem. Phys., 2016, **18**:6252 [Crossref], [Google Scholar], [Publisher]
[56]. Chen C.S., Wan J.H., Yeo B.S., J. Phys. Chem. C, 2015, **119**:26875 [Crossref], [Google Scholar], [Publisher]
[57]. Keerthiga G., Viswanathan B., Pulikottil C.A. , Chetty R., *Bonfring Int. J. Ind. Eng. Manag. Sci*., 2012, **2**:41
[58]. Andrews E., Ren M., Wang F., Zhang Z. , Sprunger P., Kurtz R., Flake J., *J. Electrochem. Soc*., 2013, **160**:H841 .[Google Scholar], [Publisher]
[59]. Lv W., Zhou J., Bei J., Zhang R., Kong F., and Wang W., *Int. J. Electrochem. Sci.*, 2016, 6183 [Crossref], [Google Scholar], [Publisher]
[60]. Tang Q., Lee Y., Li D.-Y., Choi W., Liu C.W., Lee D., Jiang D., *J. Am. Chem. Soc.*, 2017, **139**:9728 [Crossref], [Google Scholar], [Publisher]
[61]. Kim D., Xie C., Becknell N., Yu Y., Karamad M., Chan K., Crumlin E.J., Nørskov J.K., Yang P. *J. Am. Chem. Soc.*, 2017, **139**:8329 [Crossref], [Google Scholar], [Publisher]

How to cite this manuscript: Pigewh Isa Amos, Hitler Louis, Kayode Adesin Adegoke*, Ededet Akpan Eno, Akakuru Ozioma Udochukwu, Thomas Odey Magu. Understanding the mechanism of electrochemical reduction of CO2 using Cu/Cu-based electrodes: A review *Asian Journal of Nanoscience and Materials*, 2022, 5(4), 252-293. DOI: 10.26655/AJNANOMAT.2022.4.2